ABSTRACT

Jackson III, Willard B. **Heat Transfer Augmentation via Microencapsulated Phase-Change Material.** (Under the direction of Dr. Richard D. Gould)

Results disclosed in this thesis indicate that a microencapsulated octacosane phase-change material fluid is well suited for large scale electronic cooling applications. The fluid was successfully circulated in a liquid pumped loop heat exchanger system resembling the cooling system of an electric vehicle. Little or no particle breakdown occurred to the polymer encapsulated spheres. The high melting point, $T_{melt} \sim 60°C$, of octacosane PCM make it ideal for cooling electronics. The microPCM fluid is controllable by using a pump at all times. To achieve optimum performance from the microPCM fluid, the concentration of solid PCM particles and the mass flow rate must be tailored to the amount of energy that needs to be transferred and the maximum surface temperature at which this can be accomplished. For the 0.0138 meter internal diameter, smooth copper tube used in the experiments, the microPCM fluid produced lower exit surface temperatures than the 50/50 ethylene-glycol/water baseline fluid for mass flow rates less than 0.035 kg/s. This flow value is independent of the applied heat rate so long as some un-melted PCM particles remain at the exit of the heated section. MicroPCM fluids should be considered as a working fluid for liquid heat transfer systems when pumping power limitations, low surface temperature or surface temperature uniformity are design requirements. When operated at the correct conditions, the enhanced heat capacity of octacosane microPCM fluid will provide lower and more constant surface temperatures, and require less pumping power than conventional coolants.

Heat Transfer Augmentation via Microencapsulated Phase-Change Material

by

Willard Bernard Jackson III

A thesis submitted to the Graduate Faculty of
North Carolina State University
in partial fulfillment of the
Requirements for the Degree of
Master of Science

Mechanical and Aerospace Engineering

Raleigh, NC

2002

APPROVED BY:

_____ _____

_____

Chair of Advisory Committee

I dedicate this work to my family.

Thanks for all the love and support through the years.

BIOGRAPHY

Willard Bernard Jackson, III, was born June 26, 1976 in Durham, North Carolina, where less than a mile away, Willard Street intersects Jackson Street. At the beginning of grade school his family moved a short distance to Raleigh. Twelve years later, in 1994, he graduated from Millbrook Senior High School. During those twelve years he enjoyed and excelled in competitive swimming.

He entered college in the fall of 1994. After completing cooperative education work designing cellular phones with Ericsson, he received a Bachelor's of Science degree in Mechanical Engineering from North Carolina State University in June of 2000.

After earning his B.S. degree, he immediately began his graduate studies at North Carolina State University, concentrating on heat transfer. While performing research for a project funded by the Department of Energy at the Applied Energy Research Laboratory, he supported himself by teaching labs and conducting research.

ACKNOWLEDGEMENTS

The author wishes to extend his sincere appreciation to each individual that contributed to his success while at North Carolina State University. A special thanks to Dr. R. D. Gould for his advice and guidance through the research work and for chairing the advisory committee. Thanks to Dr. J. C. Mulligan for sharing his vast knowledge and advice dealing with the research material. Also, a special thanks to A. V. Kuznetsov for residing on my graduate committee. I am grateful to Yvonne Bryant of Triangle Research and Development Corporation for her work and cooperation on this project. Finally, the U.S. Department of Energy deserves sincere appreciation for supporting this research under contract DE-FC02-00EE50631.

TABLE OF CONTENTS

TABLE OF CONTENTS (continued)

LIST OF TABLES

LIST OF FIGURES

LIST OF FIGURES (continued)

LIST OF FIGURES (continued)

LIST OF SYMBOLS

A	area (m^2)
C_p	specific heat at constant pressure (J/g-K)
d	encapsulated particle diameter (microns)
D	flow tube inner diameter (m)
E	internal energy (J)
f	friction factor in smooth tube
Gz	Graetz number
h	heat transfer convection coefficient (J/s-m^2-K)
k	thermal conductivity (J/s-m-K)
L	overall length of heat section tube (m)
$\dot{m}$	mass flow rate (kg/s)
Nu	Nusselt number
p	pressure (pa)
Pr	Prandtl number
Q	heat rate (J/s)
Re_D	Reynolds number
t	time (s)
T	temperature (K)
u	fluid velocity (m/s)
V	volume (m^3)
W	work (J)
x	axial distance down tube from beginning of heat section (m)

LIST OF SYMBOLS (continued)

Xw	mole fraction
y	distance normal to flow direction (m)
Yw	mass fraction
a	thermal diffusivity (m^2/s)
µ	dynamic viscosity (cP)
?	density (kg/m^3)
p	ratio of the circumference of a circle to its diameter
t	shear stress (N/m^2)
f	solids concentration
?	shape factor
?	kinematic viscosity (m^2/s)

LIST OF SUBSCRIPTS

act	actual, calculated from $\dot{m}C_p\Delta T$ (power input absorbed by working fluid)
b	bulk
blf	baseline fluid
bulk in	fluid temperature at heat section entrance
bulk out	fluid temperature at heat section exit
c	cross section
eff	effective
hs	heat section
l	carrier liquid
m	mean
mid	midpoint
p	pump
PCM	microencapsulated PCM fluid
r	residence
s	surface
s-1…8	location of surface thermocouple
supply	measured by power transducers (global power input)
x	axial distance down tube

1. INTRODUCTION

Technologically advanced electronics require precise and efficient management of generated heat through interactions between thermal components and the surrounding environment. The functional reliability of many electrical components decreases exponentially as the component approaches its critical temperature. As the heat flux from power transistors and CPU chips continues to increase, controlling their surface temperature requires special attention. A variety of methods exist to govern thermal conditions of electronic devices such that they operate within design tolerances. Some existing techniques to enhance heat transfer are roughening of convective surfaces, adding fins, inducing swirl flow, using electric vibration devices, and introducing solids to the heat transfer working fluid[1]. However, many of these options are not cost effective and others are difficult to implement, especially to existing systems.

This thesis investigates the functionality and efficiency of using microencapsulated phase-change material (PCM) for thermal management of such systems. A microPCM fluid is basically a carrier liquid in which small capsules of microencapsulated PCM are suspended. Specifically, for this study, octacosane is the microencapsulated PCM and is suspended in an ethylene glycol / distilled water carrier solution to form a heat transfer fluid. Octacosane paraffin is used because it has a desirable melting point around 60 degrees Celsius. As a heat transfer working fluid, microPCM slurries lie between sensible fluids and fully latent fluids. The fluid possess the desired control, flow, and predictability characteristics of simple liquids, while also having the enhanced thermal capacitance and heat transfer characteristics of phase-change fluids. Properties such as viscosity, specific heat, and the operational temperature ranges of the microPCM fluid are investigated. It is

expected that the microPCM will minimize and better control source temperatures without undue increases in system size and weight, provide a more constant wall temperature across the heat input and output sections, and manage thermal systems with more flexibility and efficiency. While many applications exist for microencapsulated octacosane PCM fluids, this study concentrates on the automotive industry, using a pumped flow loop resembling that of an EV to verify the utility of the PCM fluid.

There is an increasing demand for electric and hybrid-electric vehicles (EV and HEV) in today's automotive market. EV's and HEV's characteristically exhibit higher gas mileage than that of conventional vehicles. Electric propulsion is also cleaner, since electricity is available centrally from large, efficient power plants; little or no fossil fuel is required for vehicle operation. Because of EV's characteristics, auto makers are attempting to use the potential of electric technology to meet and exceed future government requirements for efficiency and pollution.

EVs and HEVs need advanced thermal management techniques to cool vital components. For instance, the batteries, or fuel cells presently operate in the range of 60 to 110°C and electrical components like motors, actuators, and power converters are limited to operating temperatures not exceeding 70 degrees Celcus.[2] Power semi-conductor devices are of paramount importance to EV's and are also especially sensitive to thermal failure. Because we ask the EV to perform the same basic task as a regular internal-combustion powered vehicle, we expect the overall power consumption of both vehicles to be near the same magnitude. Thermostats for internal combustion engines are typically set at about 95°C. While overall power needs of both vehicles remain equal, the EV must operate, on average, some 25°C cooler than an internal combustion engine to keep electrical components

from burning out. The low operating temperature needed for the power semi-conductors limit the temperature differential between source and sink. The diminished potential temperature gradient requires increased coolant flow rates, heat exchanger sizes, and pumping power. Current automotive pumped cooling systems using a conventional working fluid will experience increased cost, size, weight, and power requirements to adequately cool the system. A coolant exhibiting a higher heat transfer coefficient and thermal capacitance, which can be circulated through a conventional heat exchanger loop consisting of a radiator, fan, heater-core, and circulation pump is desired. It is also thought that the thermal stability of PCM fluid could increase the efficiency of heat energy recovery used by the vehicle's cabin heater. As well as having non-corrosive characteristics, the coolant must also possess similar chemical and electrochemical properties as conventional automotive coolants. A fluid composed of ethylene-glycol / water carrier solution with suspended microencapsulated octacosane based phase-change material particles can potentially provide the desired results for this application.

2. BACKGROUND

For the microPCM fluid to provide greater heat transfer and have a higher effective specific heat, a phase-change must take place within the microencapsulated spheres. The PCM must melt and freeze across the heat source and sink sections of the loop, respectively. A phase-change allows release or absorption of large amounts of latent heat during a transition of physical state. The phase-change material selected, usually paraffin, determines the melting temperature of the microPCM particles.

In 1932, Douglas received credit for inventing the first heat transfer storage system using PCM in a liquid flow loop. Designed for residential heating applications, the loop would "charge" the PCM during off-peak hours and deliver the energy in the form of heat during peak electrical hours.[3] Likewise, Newton received patents in 1944 for applications tailored toward harnessing incident solar heat energy by using PCM.[4] During the 1960's, NASA funded Dr. Telkes at the Massachusetts Institute of Technology to develop PCM fluid in heat transfer devices used to cool spacecraft navigation computers.[5] This project began a string of projects funded for PCM applications dealing with state-of-the-art space-grade electronics. Research in thermal energy storage using PCM began at North Carolina State University in 1975 when Bailey and Mulligan carried out an investigation on the use of PCM for solar heating and cooling applications.[6,7] During 1982, Mulligan studied the use of PCM in heat pump systems.[8] Since then, North Carolina State University, often teamed with Triangle Research and Development Corporation, has been heavily involved in PCM fluid research.[9-17] A brief list of other recent publications on this subject include: Roy and Sengupta[18], Kasza and Chen[19], Charunyakorn[20], Manish[21], Fossett and Maguire[22], and Yasushi[23].

3. INVESTIGATION OBJECTIVES

This proof-of concept investigation focuses on experimentally verifying and quantifying the improvement in thermal management of automotive EV and HEV systems that a microPCM fluid provides over a conventional working fluid. Possessing the most potential for augmented heat transfer in this application, microencapsulated octacosane carried by ethylene-glycol/water fluid is the particular microPCM candidate chosen for the study. Specifically, experimental investigations using a pumped loop will attempt to show that the microPCM fluid exhibits elevated convection coefficient values, increased effective specific heat, and a lower fluid temperature increase across the heat source, yielding reduced wall surface temperatures when compared with the baseline ethylene-glycol/water solution. The viscosity of the microPCM fluid is determined experimentally. Since the viscosity of the PCM fluid is higher than that of the conventional baseline working fluid, required pumping power to remove heat energy is also considered.

Thermal and flow properties of this fluid are experimentally determined using a Saybolt viscometer and a bench-scale pumped loop. The loop allows direct comparison of the performance of the microPCM fluid to the simple baseline fluid under true working conditions. This evaluation quantifies the efficiency of the microPCM and identifies possible problems such as breakdown of the polymer encapsulation material from pumping and non-equilibrium conditions due to the densities of the PCM fluid components. An attempt is made, when possible, to verify results with published heat transfer correlations. This work provides a measurement of the utility of using microPCM as a cooling strategy for EV and HEV applications.

4. WORKING FLUID PROPERTIES

Flow rate, heat exchanger geometry, and the working fluid circulated in a forced convection, liquid cooling system will determine the performance of the system. This chapter presents properties of the two working fluids compared in this investigation.

4.1 Ethylene-Glycol / Water Baseline Properties

Single-phase fluids have been researched sufficiently and tabulated values of their thermophysical and thermodynamic properties are published. The fluid properties for ethylene-glycol and distilled water are widely published. The baseline ethylene-glycol/water fluid is a solution composed of equal volumes of ethylene-glycol and water, a 50/50 by volume solution. Procedures for combining the two components used in this analysis were found in AIChE[24]. The constituent properties were combined by mass fraction, Yw, for specific heat, C_p and mole fraction, Xw for viscosity, μ and thermal conductivity, k. Table 1 gives property values of the 50/50 baseline solution at various temperatures.

Table 1: Thermophysical properties of 50/50 by volume ethylene-glycol/water

Temp		Xw	Yw	r, sol	Cp, sol	m, sol	k, sol	n, sol	a, sol	Pr, sol
K	C	mole frac.	Mass frac	[kg/m^3]	[J/kg-K]	[kg/m-s]	[W/m-K]	[m^2/s]	[m^2/s]	
295	21.85	0.76	0.48	1063.59	3242.76	5.62E-03	0.423	5.28E-06	1.23E-07	4.30E+01
300	26.85	0.76	0.48	1059.96	3253.03	4.62E-03	0.427	4.36E-06	1.24E-07	3.52E+01
305	31.85	0.76	0.48	1056.30	3263.50	3.85E-03	0.430	3.64E-06	1.25E-07	2.92E+01
310	36.85	0.76	0.48	1052.61	3274.17	3.23E-03	0.433	3.07E-06	1.26E-07	2.44E+01
315	41.85	0.76	0.48	1048.89	3285.07	2.74E-03	0.436	2.62E-06	1.27E-07	2.07E+01
320	46.85	0.76	0.48	1045.14	3296.21	2.35E-03	0.439	2.25E-06	1.27E-07	1.76E+01
325	51.85	0.76	0.48	1041.36	3307.61	2.03E-03	0.441	1.95E-06	1.28E-07	1.52E+01
330	56.85	0.76	0.48	1037.55	3319.28	1.77E-03	0.444	1.70E-06	1.29E-07	1.32E+01
332	59	0.76	0.48	1036.01	3324.03	1.67E-03	0.445	1.62E-06	1.29E-07	1.25E+01
332.5	59.5	0.76	0.48	1035.63	3325.23	1.65E-03	0.445	1.60E-06	1.29E-07	1.23E+01
335	61.85	0.76	0.48	1033.70	3331.24	1.55E-03	0.446	1.50E-06	1.30E-07	1.16E+01
340	66.85	0.76	0.48	1029.81	3343.51	1.37E-03	0.448	1.33E-06	1.30E-07	1.02E+01
345	71.85	0.76	0.48	1025.89	3356.10	1.22E-03	0.450	1.19E-06	1.31E-07	9.07E+00
350	76.85	0.76	0.47	1021.93	3369.02	1.09E-03	0.452	1.06E-06	1.31E-07	8.12E+00
355	81.85	0.76	0.47	1017.94	3382.30	9.80E-04	0.453	9.62E-07	1.32E-07	7.31E+00
360	86.85	0.76	0.47	1013.91	3395.95	8.87E-04	0.455	8.75E-07	1.32E-07	6.62E+00
365	91.85	0.76	0.47	1009.83	3409.99	8.07E-04	0.456	7.99E-07	1.32E-07	6.04E+00
370	96.85	0.76	0.47	1005.72	3424.42	7.38E-04	0.457	7.34E-07	1.33E-07	5.53E+00

4.2 Microencapsulated PCM Fluid Properties

4.2.1 MicroPCM Fluid Appearance

Microencapsulated PCM fluid possesses characteristics of both a sensible fluid and a fully latent fluid. Fluid with the correct mixture of PCM particles will have the needed control, flow, and predictability of simple fluids while also having enhanced thermal capacitance and heat transfer attributes of phase-change fluids.

Triangle Research and Development Corporation mixed the microPCM fluid used in the investigation. TRDC also added 1%, by volume, of the dispersant Pluronic, L-62 manufactured by 3M. Though the dispersant affects the heat transfer properties of the fluid very little, it provides a noticeable decrease in viscosity. From TRDC's records, the microencapsulated octacosane particles used to mix the fluid came from batch M46-03.

TRDC also disclosed that the particles have a diameter of 10-30 microns with a mean particle diameter of 20 microns. The polymer shell encapsulating the PCM has a wall thickness of approximately 1 micron. Because of viscosity and expected thermal capacity, the particle concentration selected for testing in the loop, was 23% by weight. At the chosen 23 % particle/carrier mixture, the microPCM fluid has a creamy, milky consistency.

While pumped in the loop, the PCM fluid remains an aqueous mixture at all times, regardless of the phase of the PCM. However, if left un-circulated for a period of more than 24 hours, the PCM fluid will stratify. This occurs because the density of the particles is slightly less than that of the carrier solution. Once stratification is complete, the particles conglomerate at the top surface of the PCM fluid container and the carrier solution resides below. The particles mix with the carrier solution easily when the PCM fluid sits less than one week. When the PCM fluid remains at rest for extended periods of time over one week,

intentional mixing is required to integrate the particles back into the carrier solution. Figure 1 below shows the microPCM fluid, in a mixed flow condition, magnified by an optical microscope.

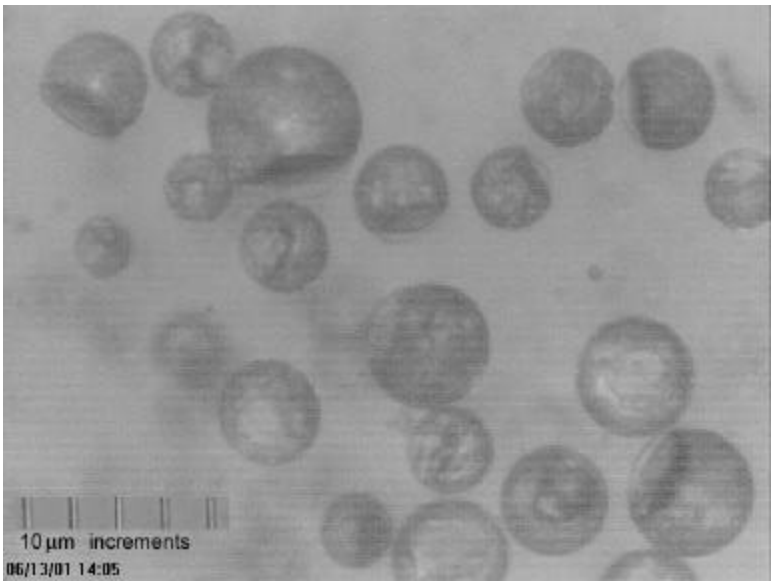

Figure 1: Microencapsulated octacosane PCM fluid, 23 percent by weight

4.2.2 Differential Scanning Calorimeter Data

Triangle Research and Development Corporation, who supplied the microPCM fluid, also measured the properties of non-encapsulated bulk octacosane paraffin using a Perkin-Elmer differential scanning calorimeter. This machine gives the energy storage of the sample per unit weight of the sample. The test was run, heating the bulk PCM from 30.0°C to 80.0°C at a rate of 5.0°C per minute. The result of this experiment is shown in figure 2. The sample weight tested in this experiment was 1.840mg. The heat energy storage capacity of the bulk octacosane PCM when no phase occurs is 49.9mW. During the solid to liquid phase change, the peak energy storage increases to 65.4mW. This shows a difference of 15.5mW in the energy storage capacity of the bulk PCM due to the latent energy storage capacity.

Thus, the thermal energy storage capacity of the non-encapsulated, bulk octacosane paraffin, when undergoing phase-change is 259.1 Joules/gram.

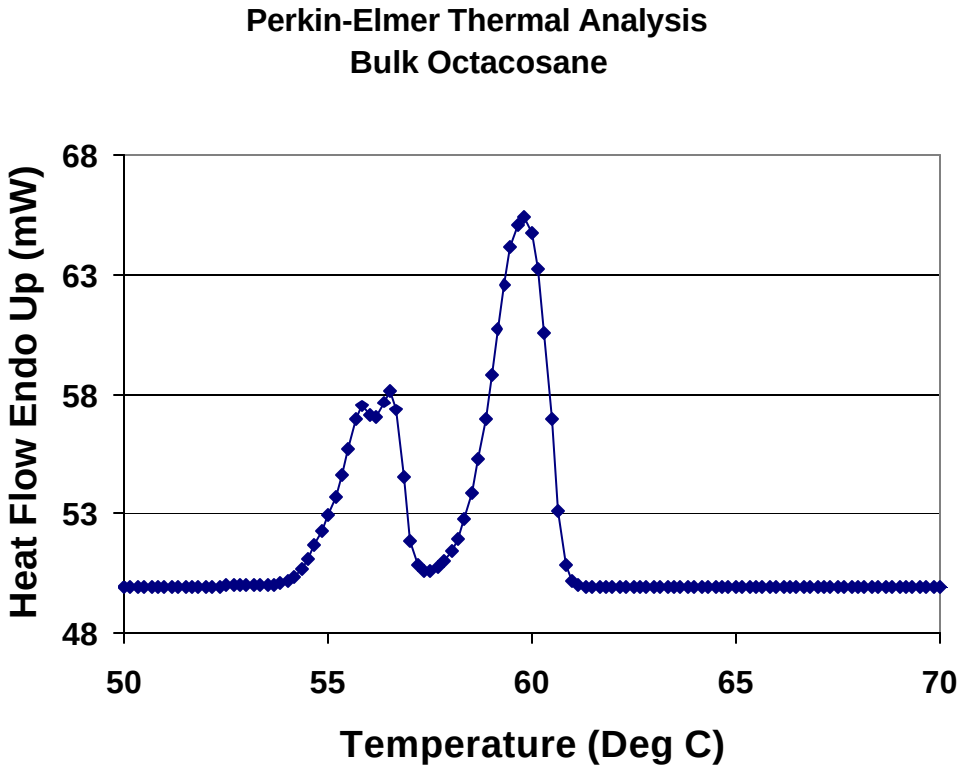

Figure 2: DSC data for bulk octacosane

The same test was run on the octacosane once it was encapsulated and suspended in the ethylene-glycol/water carrier fluid to form a microPCM fluid. These results are presented in figure 3. From figure 3, it is apparent the PCM fluid's conduction has decreased slightly from that of the bulk octacosane, because the curve is gentler and spread out; attributed to the polymer shell containing the PCM and the carrier solution. Nevertheless, the solid to solid and solid to liquid phase-change is evident. This sample weight was 75.57mg. The energy storage capacity of the microPCM fluid when no phase change occurs is 68.6mW. When the solid to liquid phase change occurs, the thermal energy storage capacity increases to

110.3mW. This yields an increase of 41.7mW from the latent storage capacity of the microencapsulated particles. Thus, the thermal energy storage capacity of the microPCM fluid is 49.4 Joules/gram while in the phase change region; this is the effective heat of fusion.

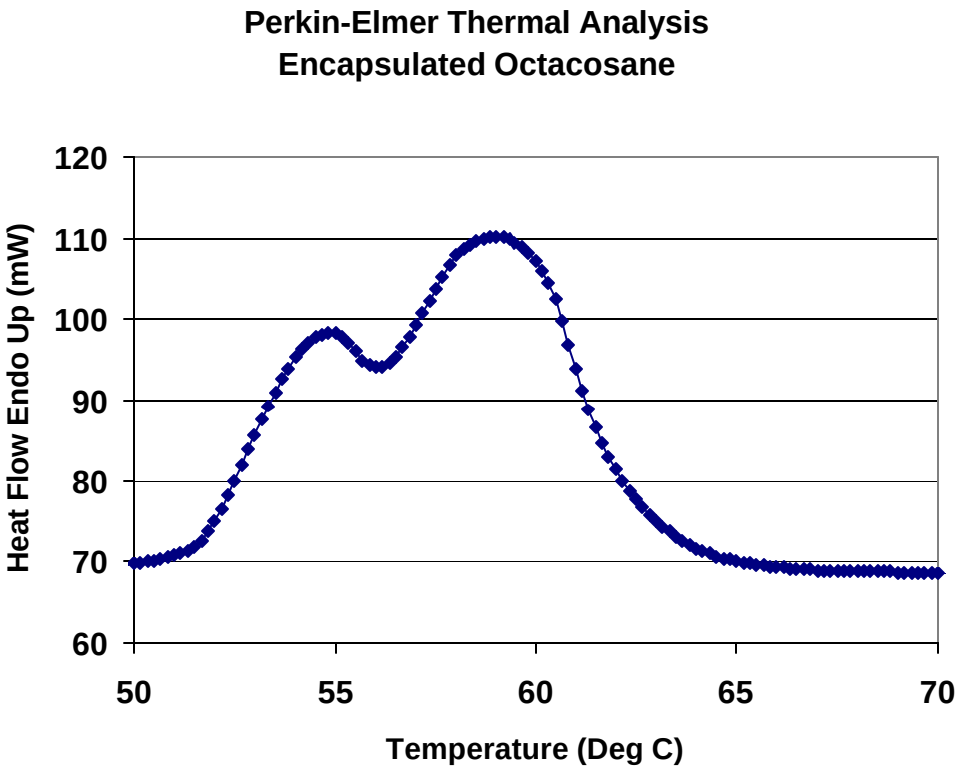

Figure 3: DSC data for 23% concentration octacosane microPCM fluid

The PCM fluid was also tested in the Perkin-Elmer DSC after it was run in the pumped loop for 50 plus hours. The results were very similar to the results of the new, unused PCM fluid. This indicates the microencapsulated particles did not rupture during use in the pumped loop and retained their original ability to absorb latent heat energy. No evidence of polymer shell breakdown, such as free wax in the PCM fluid, occurred during this investigation.

4.2.3 Viscosity

The viscosity of a microPCM fluid is critical to heat transfer performance as a function of pumping power. Fluid viscosity determines how difficult it is to pump or pour the fluid. It measures the resistance to the bulk motion of flow. This resistance occurs from friction between fluid molecules caused by the no-slip boundary condition. The no-slip boundary condition states that a moving fluid in contact with a stationary surface assumes zero velocity at the surface. Viscosity is an extremely temperature dependent property. Newton is credited for relating the shear stress, t, for a laminar flow to dynamic viscosity, μ, fluid velocity, u, and position from the stationary surface, y as:

$$t = m\frac{du}{dy} \tag{4.2-1}$$

Newtonian fluids exhibit a linear shear stress dependence on the velocity gradient and follow the relationship in 4.4-1. Core[9] experimentally studied the fluid viscosity of microencapsulated eicosane and octadecane. This study found that over the useful temperature range, PCM fluids with up to 35 percent solid mass concentrations exhibit Newtonian behavior.

Wallis[25] offered an experimentally verified correlation for microPCM fluid viscosity with 25 percent or less solid mass particle concentration. The correlation that defines the viscosity for two-component microPCM fluid is given by:

$$m_{PCM} = m_l e^{w} \tag{4.2-2}$$

where μ_{PCM} is the microPCM fluid viscosity and μ_l is the carrier fluid viscosity. To find ?, given in equation 4.4-3, the particle diameter in microns, d, must be known. For Newtonian

fluids, the shape factor, ?, is given as unity. The concentration of microencapsulated particles in the two-component fluid is represented by f, and thus

$$w = f\left(2.5 + \frac{14\Psi}{d^{0.5}}\right) \tag{4.2-3}$$

Demonstrated below, the Wallis correlation fits experimental microPCM fluid data closely.

The viscosity of the 50/50 by volume ethylene glycol/water baseline fluid and octacosane microPCM fluid with concentrations of 10, 18, 23, and 28 percent by weight PCM particles were experimentally measured over the useful operating temperature range. The viscosity of the microPCM fluid proved very temperature dependent. The microPCM fluid was heated to a homogenous temperature while it was simultaneously stirred. Then it was immediately put into the viscometer and the viscosity measured. These measurements were taken using a Saybolt viscometer and the results are provided in figure 4.

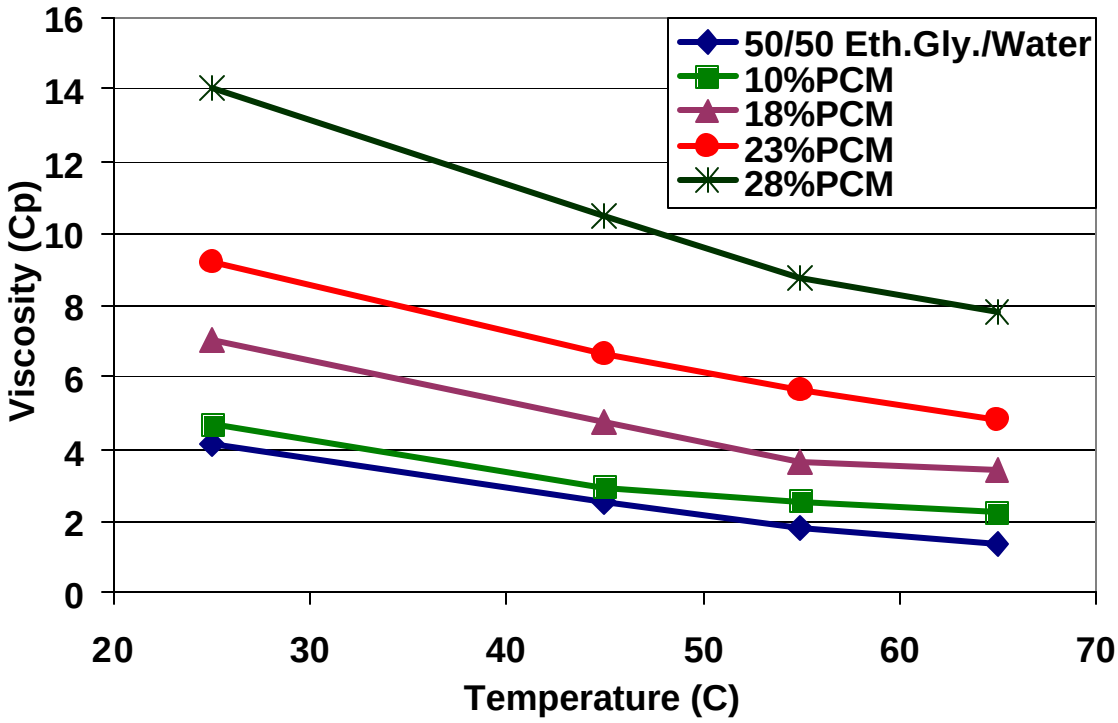

Figure 4: Viscosity temperature dependency measured via a Saybolt viscometer

At a working fluid temperature of 60°C, the viscosity of the 23 percent solid fraction microPCM suspension fluid is 3.5 times greater than the baseline fluid viscosity. The Wallis correlation predicts that the microPCM fluid viscosity will be 3.6 times greater than the baseline fluid viscosity at these conditions. Elevated viscosity is undesirable, as pumping power must be increased to sustain a given flow rate. To maintain identical Re_D, increased pumping power is required for the microPCM fluid and must be considered when comparing the performance of these coolants.

Figure 5 shows that the viscosity of the microPCM fluid increases exponentially with increased solid particle fraction as indicated by the Willis equation, but the fewer PCM particles in the microPCM fluid, the less latent heat capacity the fluid will possess.

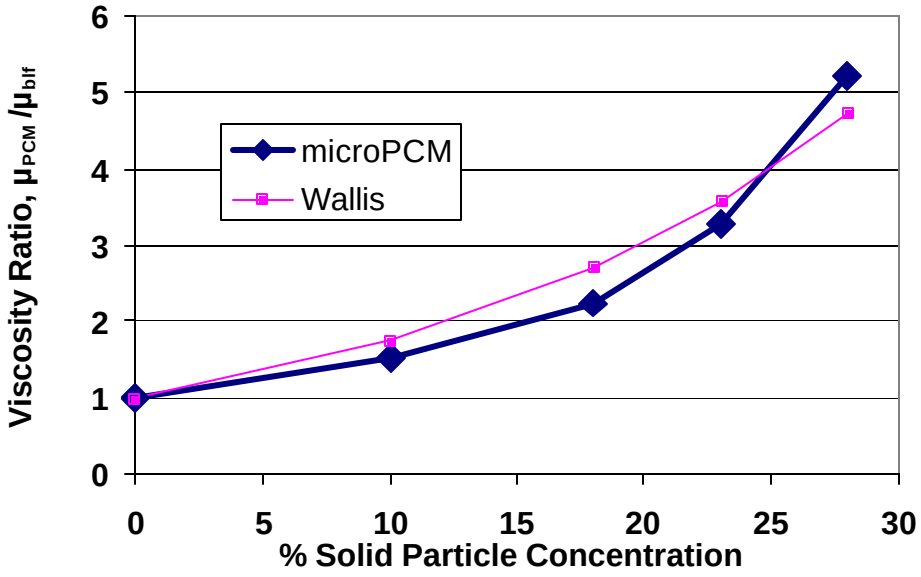

Figure 5: Viscosity dependency of solid particle concentration at 60°C

However, the change in latent heat capacity of the microPCM fluid has a one to one relationship to particle concentration. The solid particle fraction appears to decrease the

sensible heat capacity of the microPCM fluid by a little less than half the solid particle fraction when the fraction is less than 28 percent. So a 23 percent solid particle fraction reduces the sensible heat capacity by approximately 11.5 percent.

4.2.4 Density

The density of the baseline fluid was calculated using tabulated data and verified experimentally. The density of the microPCM fluid was experimentally determined. Though particle concentration and average particle diameter was known, the density and exact thickness of the polymer encapsulating material was not. Furthermore, as can be seen in figure 1, when the octacosane is solidified, many of the particles are not completely full of PCM. This makes it difficult to accurately predict the density of the microPCM fluid. Even so, the theoretical density of the microPCM fluid was estimated by percent weight of concentration of PCM solid in the fluid, using 803 kg/m^3 as the density of octacosane at 21°C. The density of the ethylene-glycol/water baseline is tabulated in table 1. This estimation under predicts the microPCM fluid density, ignoring the mass of the encapsulation material. The equation used to predict the theoretical density is

$$r_{PCM} = (1-f)r_{blf} + f r_{octacosane} \tag{4.2-4}$$

To find experimental densities, a laboratory grade 50 ml Erlenmeyer flask was tarred on electronic scales. The flask was filled with fluid and the fluid's mass was recorded. Thus the density was found from the volume and mass measurements. Table 2 gives experimental and theoretical density for the 50/50 baseline and four selected microPCM particle concentrations at 21°C. Notice the encapsulated microPCM particles are less dense than the ethylene-glycol/water carrier solution. This causes some stratification when the microPCM

fluid sits undisturbed for extended periods of time. Figure 6 shows the temperature dependency of the 50/50 ethylene-glycol/water baseline fluid and the 23 percent particle concentration microPCM fluid.

Table 2: Experimental density at 21°C

Particle concentration, f_s kg / m^3	Eth/H_20	10%	18%	23%	28%
Experimental	1063.5	1054.1	1051.6	1046.7	1043.8
Theoretical	1063.59	1037.54	1016.69	1003.66	990.63

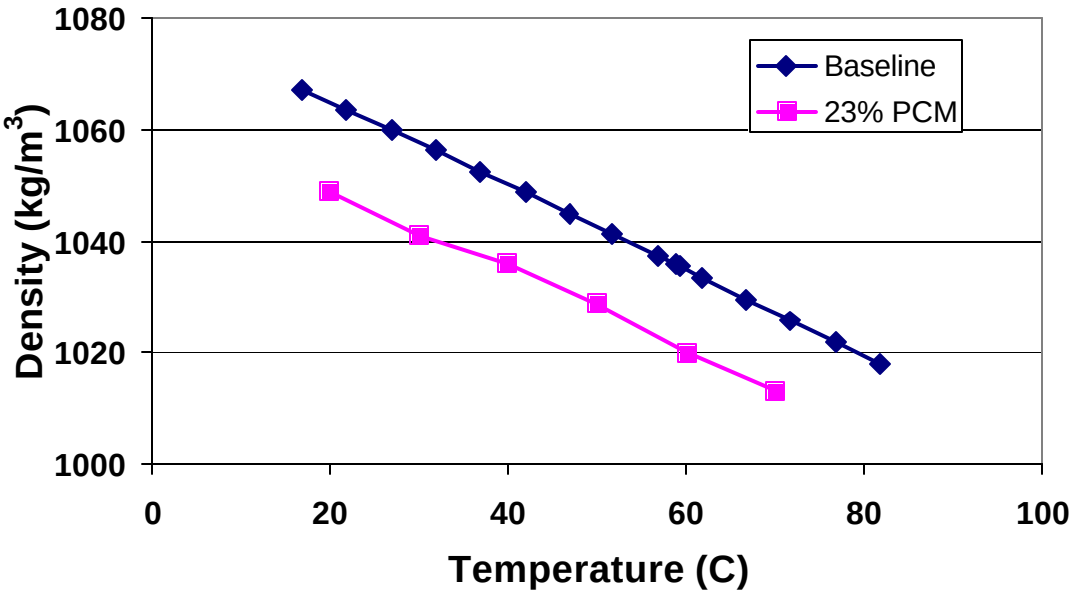

Figure 6: Density of working fluids over useful temperature range

5. TEST FACILTIY

A fully instrumented bench-scale flow loop was constructed to validate the use of an octacosane microPCM fluid for EV and HEV electronics cooling. A schematic of the thermal test loop is shown in figure 7.

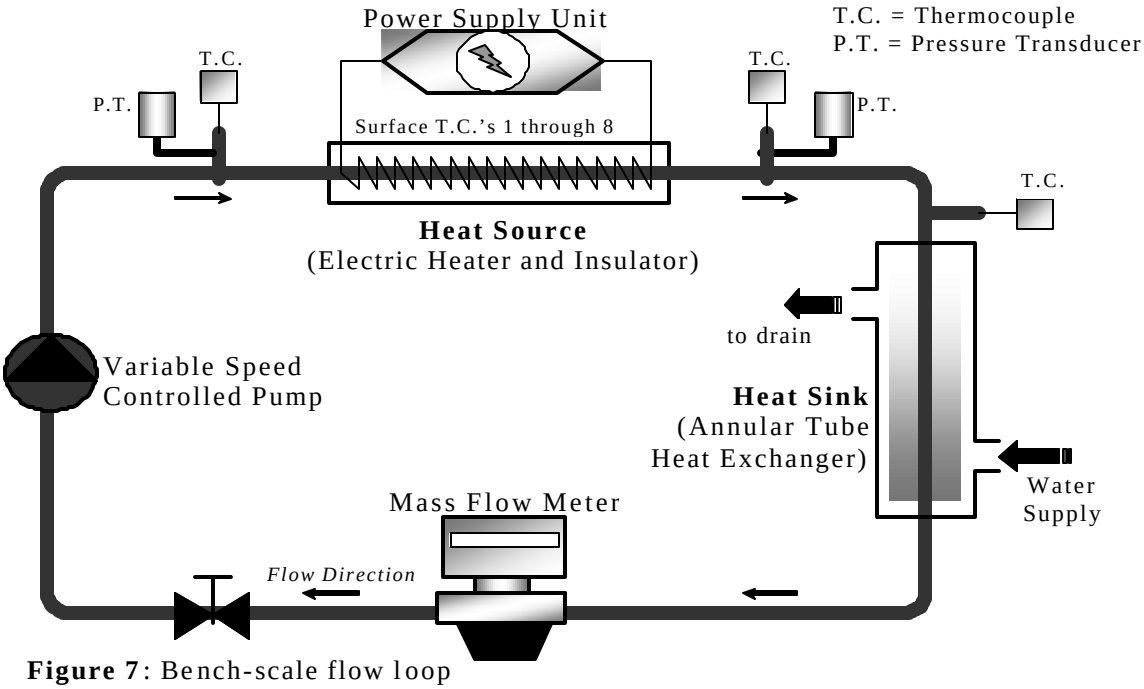

Figure 7: Bench-scale flow loop

The bench-scale loop was designed to model the cooling of a heat dissipating electronic component in an EV; however, the entire loop was insulated so as little free convection as possible occurred to the environment. To model the heat source side, a 1.804 meter long copper tube, with an inner diameter of 0.01384 meters, was wrapped evenly with four identical electrical heating tapes. The outer surface of the heating tape was insulated with fiberglass and foil insulation so that virtually all of the heat flows into the tube and working fluid. At each end of the heated copper tube heat section, a 2 inch long PVC hot water pipe,

with the same diameter as the copper tube, was placed inline to combat axial heat conduction. Omega thermocouple probes (6" length, 304 S.S. 0.062" sheath diameter, part no. TMQSS-062U-6) were used to measure the bulk temperature of the working fluid at three critical points around the loop. Eight self-adhesive thermocouples (type T: Copper-Constantan, 0.010 diameter with teflon insulation, part no. PL110102) were affixed along the outer surface (between the heat tape and the tube) of the copper tube heat source section at evenly spaced intervals. A close-up of the heated section, with fluid and surface thermocouple locations, is shown in figure 8.

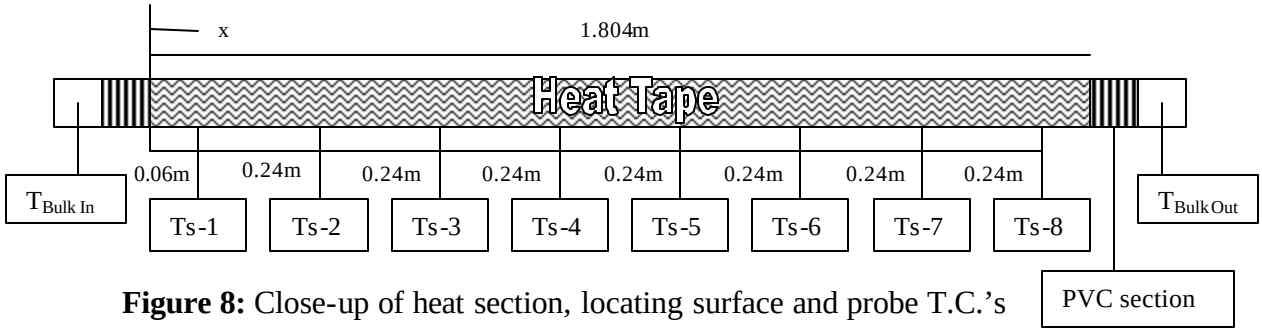

Figure 8: Close-up of heat section, locating surface and probe T.C.'s

Four Omegalux® heavy-duty electrical heater tapes (part no. STH051-060) were connected to a potentiometer that provided a constant controllable heat flux to the heated section from 0 to 600 Watts. The heating tape simulates heat dissipated by common EV power components. Two Omega watt transducers (part no. O10-51580AFA0) were used to measure the total power dissipated by the heating tapes. Two high accuracy Omegadyne pressure transducers (Part No. PX01C1-050AV) later replaced by a differential water manometer, were used to measure the pressure drop across the heat source section.

A 65-watt variable speed Laing Recirc® pump (Model No. SM-605-BTW) was used to control the fluid flow rate. This is a magnetically coupled pump, so there are no seals. This pump was designed for recirculation of hot water in residential buildings, so the relatively

low RPM operation combined with the magnetically coupled centrifugal rotor made it ideal for pumping microPCM fluids.

A Micro-Motion® mass flow meter (Model No. R025SI319U) and Micro-Motion® transmitter (Model No. IFT9703IC6D3U) were used to measure the mass flow rate to within ±1%. A liquid cooled heat exchanger was used for the heat sink in this study, as this study focused on the source side heat exchanger. All transducers, thermocouples and the flow meter described above were interfaced to a Hewlett Packard Agilent 34970A data acquisition switch unit via an Agilent 34902A 16 channel multiplexer. The Agilent 34970A data acquisition unit was interfaced to a PC using a National Instruments IEEE 488 data acquisition card. A list of the data output from the flow loop to the data logger's bench-link program is listed in table 3.

Table 3: Listing of output from the flow loop to H.P. Agilent 34970A data acquisition switch

Channel #	**Measurement Type**
101	Qin to the first two heat tapes
102	Qin to the second two heat tapes
103	Mass flow rate
104	$T_{bulk\ in}$, fluid temp into the heat section
105	Pressure at beginning of the heat section
106	Pressure at the exit of the heat section
107	$T_{bulk\ out}$, Downstream bulk fluid exit temp
108	T_{out2}, Exit bulk fluid temp of heated section
109	$T_{s\text{-}1}$, Surface T.C. at x = 0.062m
110	$T_{s\text{-}2}$, Surface T.C. at x = 0.302m
111	$T_{s\text{-}3}$, Surface T.C. at x = 0.542m
112	$T_{s\text{-}4}$, Surface T.C. at x = 0.782m
113	$T_{s\text{-}5}$, Surface T.C. at x = 1.022m
114	$T_{s\text{-}6}$, Surface T.C. at x = 1.262m
115	$T_{s\text{-}7}$, Surface T.C. at x = 1.502m
116	$T_{s\text{-}8}$, Surface T.C. at x = 1.742m

6. FLOW PARAMETERS

In order to quantify the improvements yielded from the microPCM fluid when compared to an ethylene-glycol/water baseline solution, two types of tests, steady-state tests and transient tests, were run at three different heat rates. Each steady-state flow condition was conducted using a constant mass flow rate and a fixed $T_{bulk\ in}$ for each flow condition. The transient test were conducted using a constant mass flow rate, but $T_{bulk\ in}$ was allowed to increase from room temperature to about 70°C. For each flow condition, data was collected using both the 23 percent octacosane based microPCM fluid and the 50/50 by volume ethylene-glycol/water baseline solution.

6.1 Determination of Reynolds Number

The Reynolds number for internal flow, Re_D, is a dimensionless flow parameter representing the ratio of inertia and viscous forces. It is defined as

$$\mathrm{Re}_D \equiv \frac{\rho u_m D}{\mu} \tag{6.1-1}$$

For steady, incompressible flow in a tube of uniform cross-sectional area, mass flow rate and the mean velocity, u_m, are constants, independent of the length down the tube, x. Thus, knowing that $A_c = \frac{\pi D^2}{4}$ for a circular tube and $\dot{m} = \rho u_m A_c$, the Reynolds number for incompressible flow in a circular tube reduces to

$$\mathrm{Re}_D = \frac{4\dot{m}}{\pi D \mu} \tag{6.1-2}$$

Since the viscosity of the baseline and microPCM fluid are known for the flow conditions, the Reynolds number is calculated as a function of mass flow rate and is used to compare the baseline with the microPCM fluid.

6.2 Steady-state Flow Parameters and Test Matrix

All steady-state tests were conducted under the following conditions. The pumped loop, as a system, is allowed to reach thermodynamic equilibrium. The mass flow rate of the working fluid and cooling water are fixed for each test condition. The input heat rate is fixed at one of three nominal values, Q_{supply} = 600, 500, or 400 watts, applied evenly over the heat section. The cooling water at the sink heat exchanger is adjusted such that the working fluid bulk inlet temperature at the inlet to the heat section, $T_{bulk\ in}$, is 58.85°C ± 0.1°C. This temperature was chosen based on the DCS data; at 58.85°C the octacosane is in the phase-change region but still in the solid form. The octacosane will absorb the highest amounts of latent heat over the next 2°C.

Once the system has reached equilibrium at the bulk inlet temperature listed above for a given working fluid flow rate, 40 data points are taken by the data logger; one data point every 5 seconds. The 40 data points are averaged to give a data set for that working fluid flow rate. This process is repeated for each working fluid heat and flow rate listed in table 4.

Table 4: Steady-state test matrix

Tbulk In = 58.85°C ± 0.1°C					
Re_D	Baseline (kg/s)	PCM (kg/s)	600W	500W	400W
518	0.0082	0.0249	?	?	?
622	0.0099	0.0306	?		
725	0.0116	0.0381	?	?	?
829	0.0132	0.0410	?		
933	0.0149	0.0455	?		
1036	0.0166	0.0502	?	?	?
1139	0.0182	0.0559	?		
1242	0.0198	0.0601	?		
1345	0.0215	0.0656	?	?	?
1449	0.0231	0.0706	?		
1552	0.0248	0.0755	?		
1655	0.0265	0.0803	?	?	?
1758	0.0281	0.0858	?		
1862	0.0298	0.0906	?		
1965	0.0314	0.0956	?	?	?
2069	0.0330	0.1006	?		
2171	0.0347	0.1054	?	?	?
2273	0.0364	0.1105	?		
2377	0.0380	0.1156	?	?	?
2481	0.0397	0.1172	?	?	?
2584	0.0414	0.1219	?	?	?
2688	0.0429	0.1272	?	?	?
2791	0.0446	0.1321	?	?	?

6.3 Transient Flow Parameters and Test Matrix

This test situation is labeled transient because the working fluid bulk inlet temperature, $T_{bulk\ in}$, is not held constant. The test begins when the working fluid, and the entire system temperature, is well below the melting temperature of octacosane; approximately room temperature for these tests. The power to the heated section is set to a constant value, Q_{supply} = 600 watts, 500 watts, or 400 watts. The circulation pump is set so a fixed mass flow rate is maintained throughout the test period. However, the power to the pump is constantly adjusted to account for the temperature dependent viscosity effects of the working fluid. Because of changes in viscosity due to the temperature increase of the

working fluid, the Reynolds numbers range from 250 to 1500 for the baseline fluid and from 450 to 1000 for the microPCM fluid. The flow rates of the two working fluids were chosen by setting the Re_D of the two fluids equal when $T_{bulk\ in}$ equals 60°C and the viscosity is evaluated at a film temperature at the exit of the heated section.

The cooling water to the annular heat sink exchanger is always turned off for this test. Thus, no heat is removed from the system and the working fluid, through sensible or latent means, must absorb all heat entering the system. The test continues until the bulk mean inlet temperature rises from room temperature to about 70°C. Like the steady-state tests, multiple runs at comparable Reynolds numbers, calculated when $T_{bulk\ in}$ is 60°C, were chosen; they are listed in table 5.

Table 5: Transient test matrix

No Cooling Water					
Re_D	**Baseline (kg/s)**	**PCM (kg/s)**	**600 W**	**500 W**	**400 W**
933	0.0149	0.0455	?	?	?
1450	0.0231	0.0706	?	?	?
1965	0.0314	0.0956	?	?	?
2584	0.0414	0.1219	?	?	?

7. EXPERIMENTAL RESULTS

At the beginning of each day a calibration run was performed. The calibration run was conducted when the entire loop was at room temperature. Using this data, all wall surface thermocouples were referenced to the value of the $T_{bulk\ in}$ thermocouple. The $T_{bulk\ in}$ and $T_{bulk\ out}$ thermocouples were calibrated in an ice bath and a boiling bath. This process assures that the temperature readings from the system are reliable.

7.1 Heat Section Energy Balance

Using the sensible baseline fluid steady-state data, an energy balance was preformed on the heat source section of the system. This energy balance gives the quantity of Q_{supply} that actually enters the working fluid; this heat rate value is called Q_{act}. Q_{act} is determined by using parameters we know or can measure from the system such as mass flow rate and increase in the working fluid temperature across the heated section, ? T. The specific heat of the baseline, $C_{p\text{-}blf}$, is calculated by combining published tabulated specific heat values; this process was explained in section 4.1. Using these parameters,

$$Q_{act} = \dot{m} C_{p-blf} \left(T_{bulk-out} - T_{bulk-in} \right) \tag{7.1-1}$$

Since the power transducers measure Q_{supply}, we now have a measure of the quantity of heat into the system globally, Q_{supply}, and the amount of heat transferred into the working fluid, Q_{act}, in the heated section.

Figure 9 shows Q_{supply} plotted against Q_{act}. The plot indicates the heat loss from the system, over the operating range where Q_{supply} is equal to 400, 500, and 600 watts. The baseline data points for Q_{supply} values of 600 and 500 watts have less than a 10 percent error. However, some of the 400 watt data points have an error above 10 percent. All of these data points were taken on the same day. Though the errors look large, they are caused by less

than a 0.5°C fluctuation in $T_{bulk\ out}$. One calibration data set was taken on that day, but an investigation indicated the reference factors from the calibration data, used to reference all thermocouples to the $T_{bulk\ in}$ thermocouple, was the most likely cause of the increased error. Axial conduction in the working fluid accounts for much less than 1 percent of the heat loss.

Nevertheless, the average heat loss from the heated section to the environment is only 7.6 percent of the supplied heat. This value is found by dividing Q_{act} by Q_{supply} and subtracting from unity for each steady-state flow rate and taking the mean of the resulting values. For all heat rates, the error is a function of mass flow rate; the lower the flow rate, the higher the error. This value is acceptable for heat transfer experiments, and we can conclude the apparatus is functioning properly.

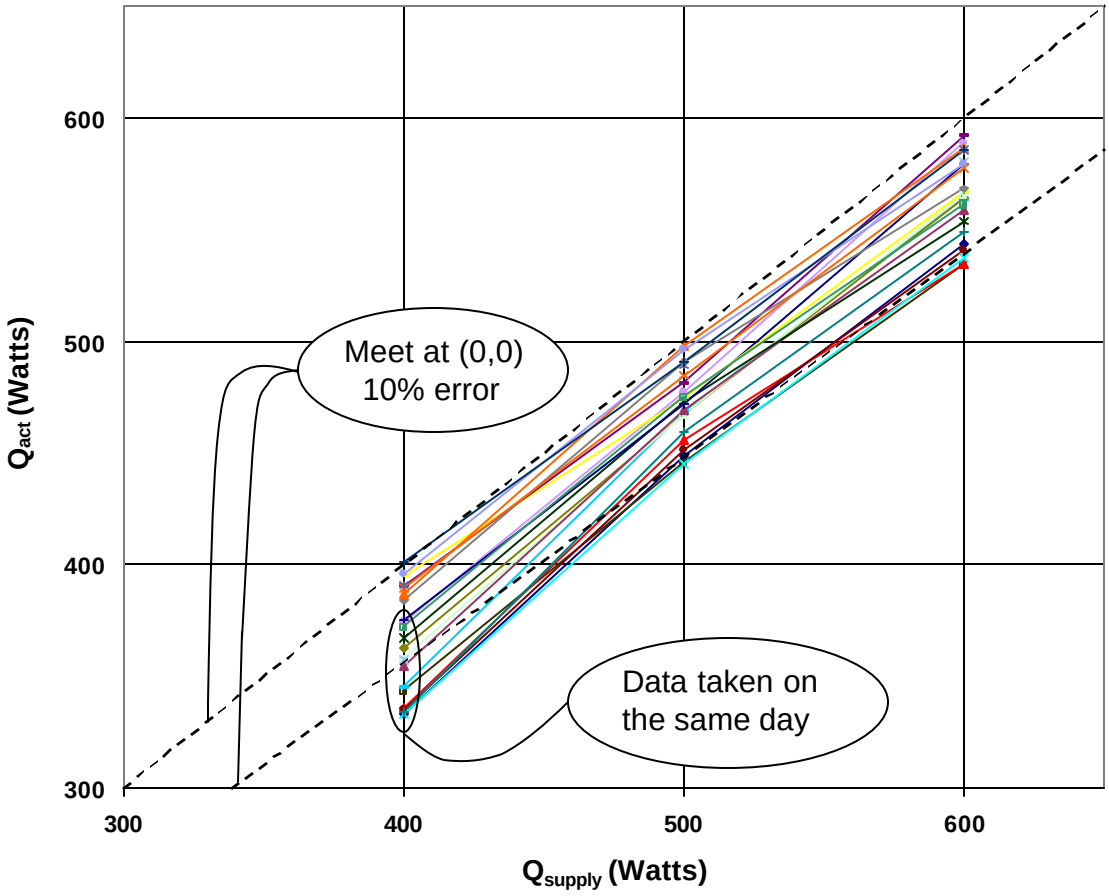

Figure 9: Q_{supply} (measured via power transducer) v. Q_{act} (m*Cp*?T)

7.2 Steady-State Results

All steady-state results are provided in tabulated form in Appendix A. For each graph in this section, every individual tick-mark data point is the result of averaging 40 measurements, taken by the data logger over a 200 second period. Each reading was taken only after the system reached equilibrium with $T_{bulk\ in} = 58.85°C \pm 0.1°C$. Heat inputs, Q_{supply}, were set to 600 watts, 500 watts, or 400 watts. All Reynolds numbers, Re_D, are a function of mass flow rate, fluid viscosity and tube diameter, outlined earlier in equation 6.1-2.

7.2.1 Axial Surface Temperature Distribution

Figures 10 through 12 show the axial surface temperature distribution along the heated section tube at the three heater supply rates for a range of laminar flow conditions. Each data point on the figures represents a surface thermocouple on the heated section tube. The specific placement and type of surface thermocouple was described earlier in the test facility section.

As expected for a purely sensible fluid, the wall surface temperature increases as the baseline working fluid travels down the heated tube. This occurs because the baseline fluid is a purely sensible fluid and the bulk fluid temperature must increase as heat energy is absorbed. As the bulk fluid temperature increases, so must the wall surface temperature, according to Newton's law of cooling.

$$Q = \bar{h}A(\bar{T}_s - \bar{T}_b) \tag{7.2-1}$$

A temperature differential large enough to transmit the applied heat energy via convection to the working fluid must be maintained.

Notice that the wall surface temperature does not increase much down the tube when the microPCM fluid is used; instead it remains controlled and nearly constant. This constant

wall temperature exists because the octacosane particles are absorbing latent heat and transporting the energy to the sink. This occurs because the PCM requires a minimum temperature differential to absorb latent heat; heat absorption is nearly isothermal during the phase change process.

Specifically, figure 10 illustrates the axial temperature distribution when Q_{supply} = 600 watts and the Re_D = 518. There is almost a 15°C decrease in wall surface temperature at x = 1.74 meters, near the exit of the heated tube when the microPCM fluid is used. That is over a 15 percent temperature reduction. Figure 11 shows the temperature distribution when Q_{supply} = 500 watts and Re_D = 518. This flow condition gives an exit wall surface temperature decrease of 11.9°C, a 13.5 percent reduction over the baseline. Figure 12 shows the distribution when Q_{supply} = 400 watts and Re_D = 518. Here an exit wall surface temperature decrease of 10.0°C occurs, which is a 12.25 percent reduction of the baseline surface temperature.

At elevated Reynolds numbers, approaching the critical value, some boundary layer viscous breakdown may occur towards the end of the heated tube, as film temperatures increase down the pipe. As noted earlier an attempt to control heat leaving the copper heat tube section via axial conduction was made by adding a 2 inch length of 0.0138 meter inner diameter PVC tube at each end of the heated section. However, some axial conduction within the 1.83m copper tube occurs. This becomes apparent as Reynolds numbers enter the transition to turbulence regime. Nevertheless, the temperature distribution down the pipe resembles analytical solutions for the baseline[16].

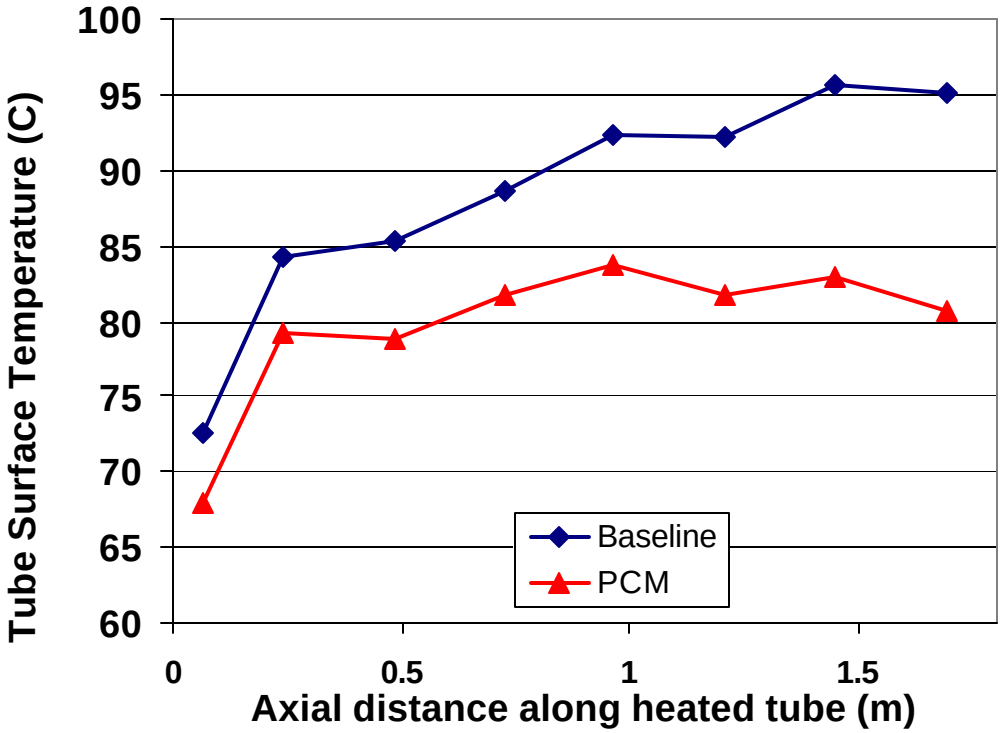

Figure 10: Surface temperature vs. tube length, x, for Re_D =518, 600 Watts

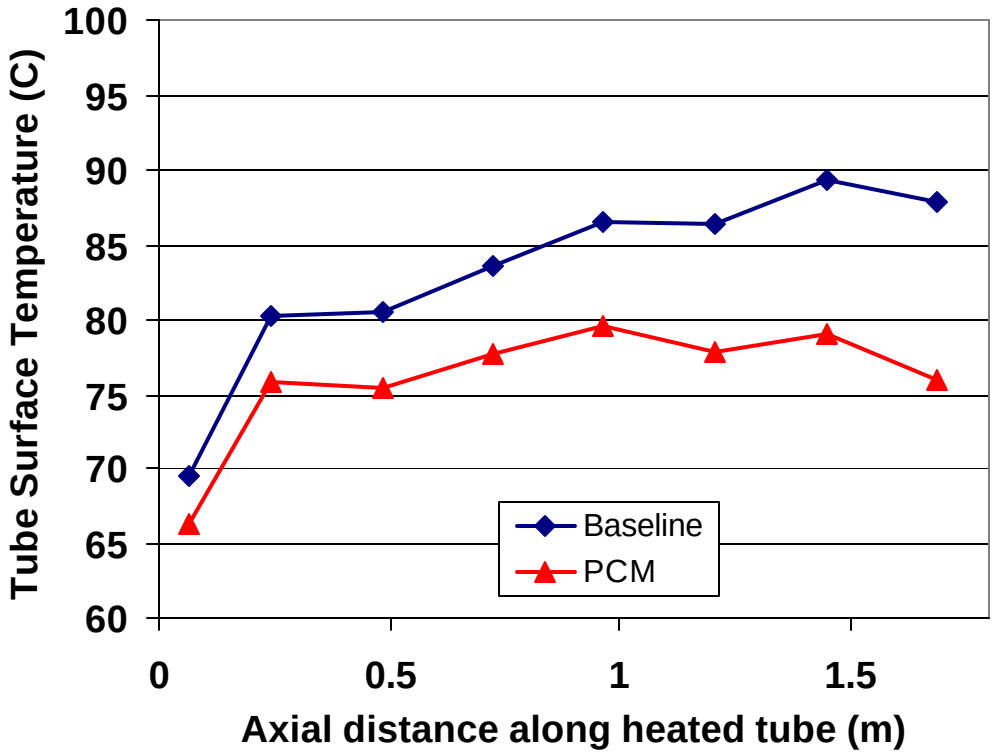

Figure 11: Surface temperature vs. tube length, x, for Re_D =518, 500 Watts

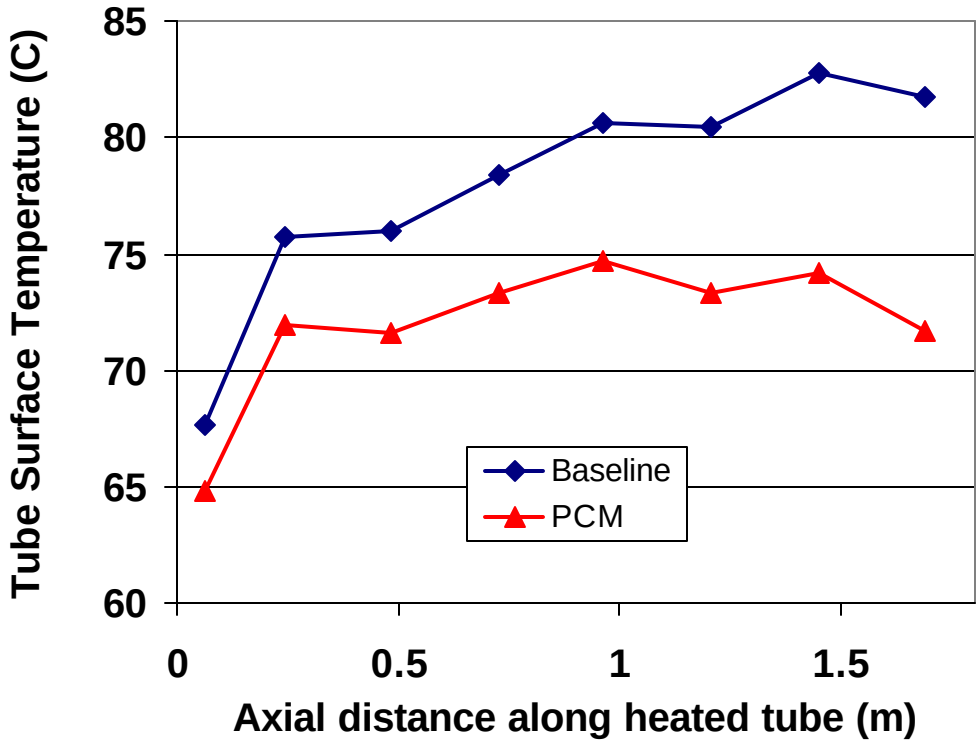

Figure 12: Surface temperature vs. tube length, x, for Re_D =518, 400 Watts

Figures 13, 14, and 15 show that the microPCM fluid continues to significantly reduce the wall surface temperature as the flow is transitioning to fully turbulent flow. Figure 13 shows surface temperatures for Re_D = 2791 and Q_{supply} = 600 watts. The surface temperature is reduced by 7.3°C at the exit of the heated tube, almost a 10 percent reduction over using the baseline fluid. Figure 14 shows the temperature distribution for Re_D = 2791 and Q_{supply} = 500; while figure 15 shows the distribution for Re_D = 2791 and Q_{supply} = 400 watts. The surface temperature is reduced by 6.1°C when Q_{supply} = 500 watts and 4.5°C when Q_{supply} = 400 watts. Note that an entry region is present and fully developed turbulence does not occur for some distance down the pipe. The wall surface temperature in the entry region will have higher temperatures than in the developed turbulent region, near the end of the tube. Though these surface temperature reductions are important, the pumping power

required to produce turbulent flow with the microPCM fluid is also significant and must be considered.

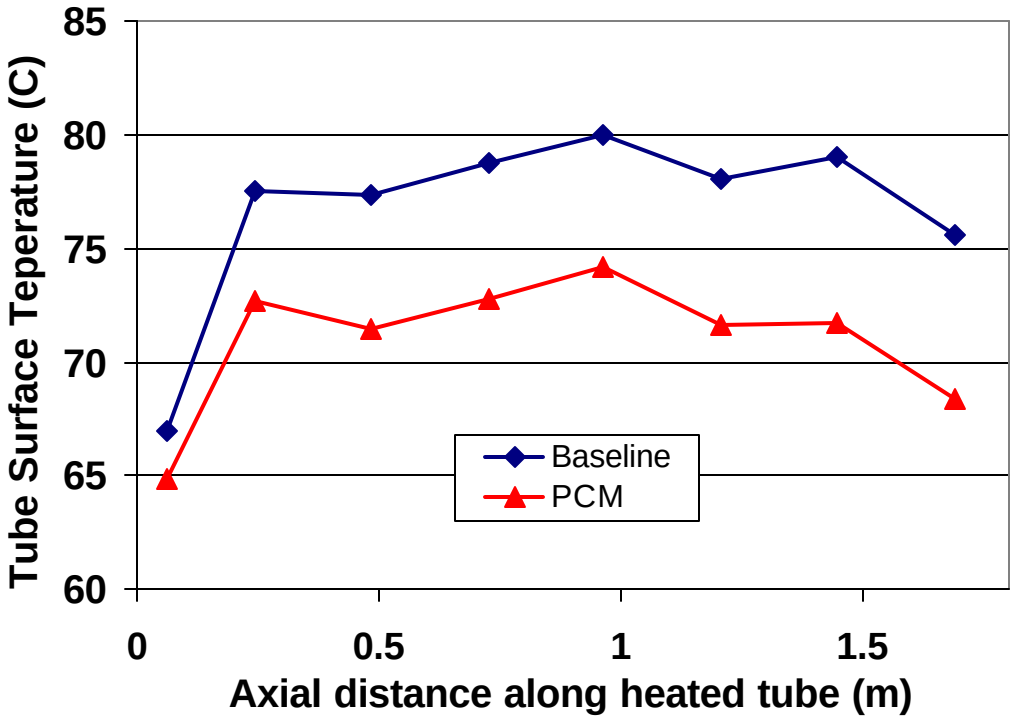

Figure 13: Surface temperature vs. tube length, x, for Re_D =2791, 600 Watts

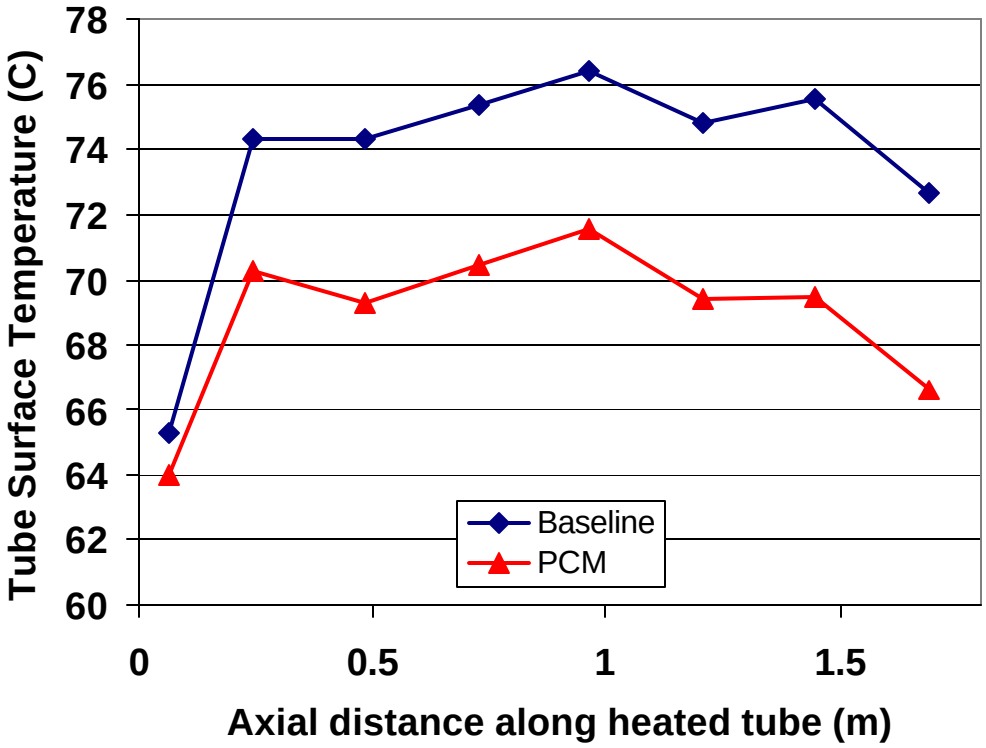

Figure 14: Surface temperature vs. tube length, x, for Re_D =2791, 500 Watts

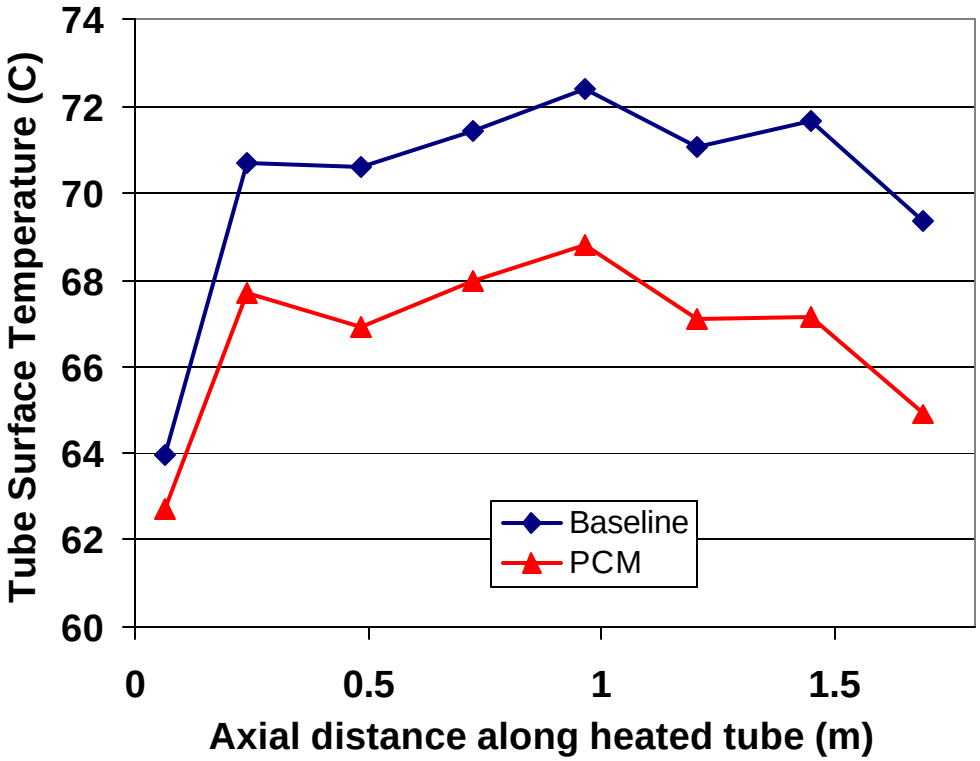

Figure 15: Surface temperature vs. tube length, x, for Re_D =2791, 400 Watts

Figure 16 depicts the percent decrease of exit wall surface temperature, T_{s-8}, for increasing laminar Reynolds numbers over the three heat rates tested. This figure indicates that the microPCM is most efficient when removal of high heat flux is accomplished at low Reynolds numbers. Not only is the percent decrease in surface temperature the greatest at low mass flow rate, but the required pumping power decreases with flow rate. As discussed earlier, surface temperatures near the exit of the heated tube become very large for single phase fluids circulating at low mass flow rates. The trade off, not represented in this figure, is that the lower the flow rate for a given heat flux, the higher the surface temperatures become.

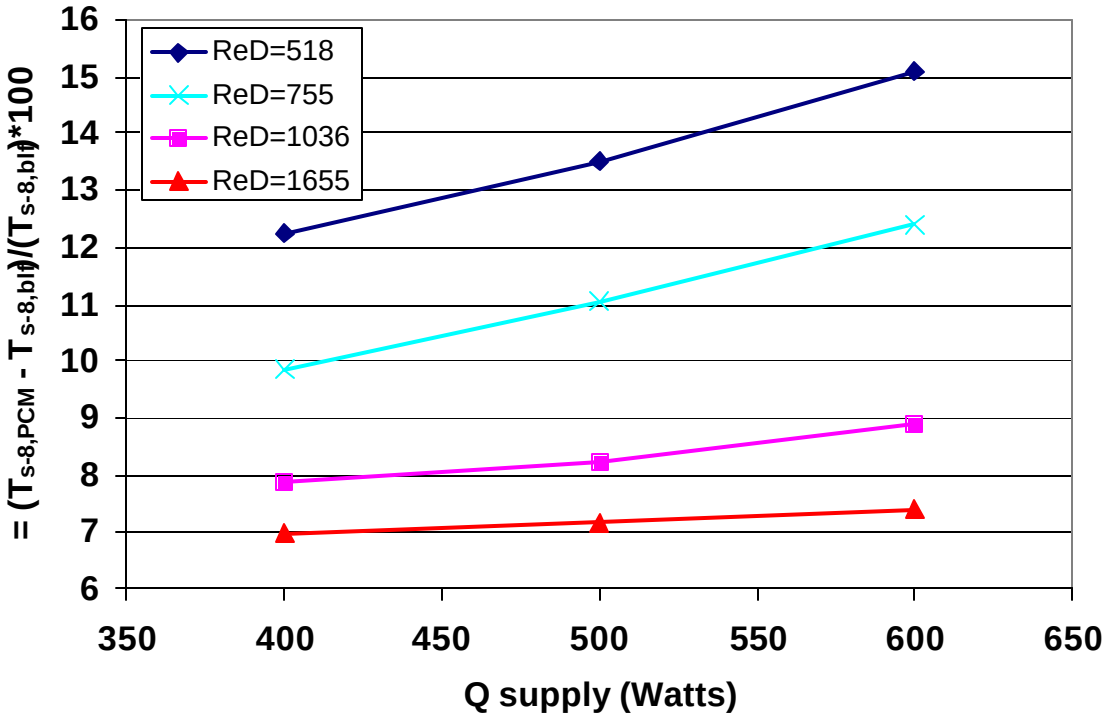

Figure 16: Percent decrease of exit wall surface temperature for laminar Re_D over heat rate

Figure 17 is similar to the axial temperature distribution, in that the curves represent wall temperatures measured by surface thermocouples. The difference is that the axial

temperature distribution plots show all eight surface thermocouples along the tube for one given Re_D, while figure 17 shows the wall entrance (x = .064m) and exit (x = 1.74m) temperatures only, but by varying the working fluid flow rate, it shows them for all laminar Re_D. The entrance thermocouple, T_{s-1} shows a slight decrease in the wall surface temperature when the microPCM fluid is used instead of the ethylene-glycol/water baseline. The exit thermocouple, T_{s-8} shows a drastic decrease in wall surface temperature when the microPCM fluid is used instead of the baseline. This occurs because the baseline working fluid must absorb all 600 watts into the sensible fluid, causing the bulk fluid temperature of the baseline to rise as it travels down the tube, making the exit temperatures extremely dependent on flow rate, or residence time. Following the Leveque convective heat transfer correlation, decreased flow rate drives down the average convection coefficient, which drives up the wall temperature along the tube so the temperature differential between the wall surface and working fluid is sufficient to absorb the heat energy applied by the heating tape.

The microPCM fluid, unlike the baseline fluid, can transport a fraction of the applied heat energy via latent heat of transformation. As the microPCM fluid travels down the tube, the octacosane undergoes a solid to liquid phase change and absorbs a fraction of the heat. This allows the wall surface temperature to remain more constant along the tube, and yields lower wall surface temperatures than the baseline fluid. Since the microPCM carrier fluid is the same sensible fluid as the baseline, the decrease in surface temperature represents the fraction of heat energy transported via of the PCM in the form of latent energy.

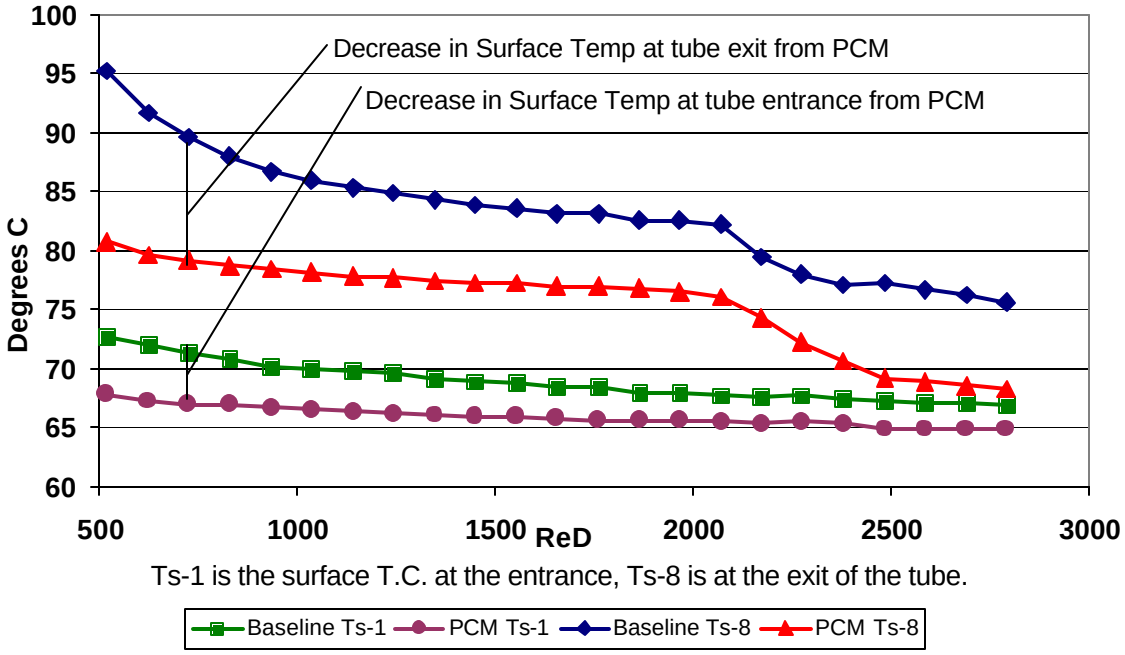

Figure 17: Entrance and exit tube wall surface temperature over Re_D

7.2.2 Bulk Fluid Temperature

When octacosane undergoes a phase change, large quantities of heat energy are absorbed or released, but no major temperature change occurs in the material. This allows the bulk fluid temperature difference across the heated section to remain small. Indeed, figure 18 shows that the fluid temperature increase across the heated section required for the microPCM fluid to transport 600 watts is only around 2°C. Interestingly, the bulk fluid temperature increase across the heated section is nearly the same when Q_{supply} is 600 watts, 500 watts, and 400 watts. This suggests that much of the heat energy is carried away by the microPCM fluid in the form of latent heat in the octacosane particles.

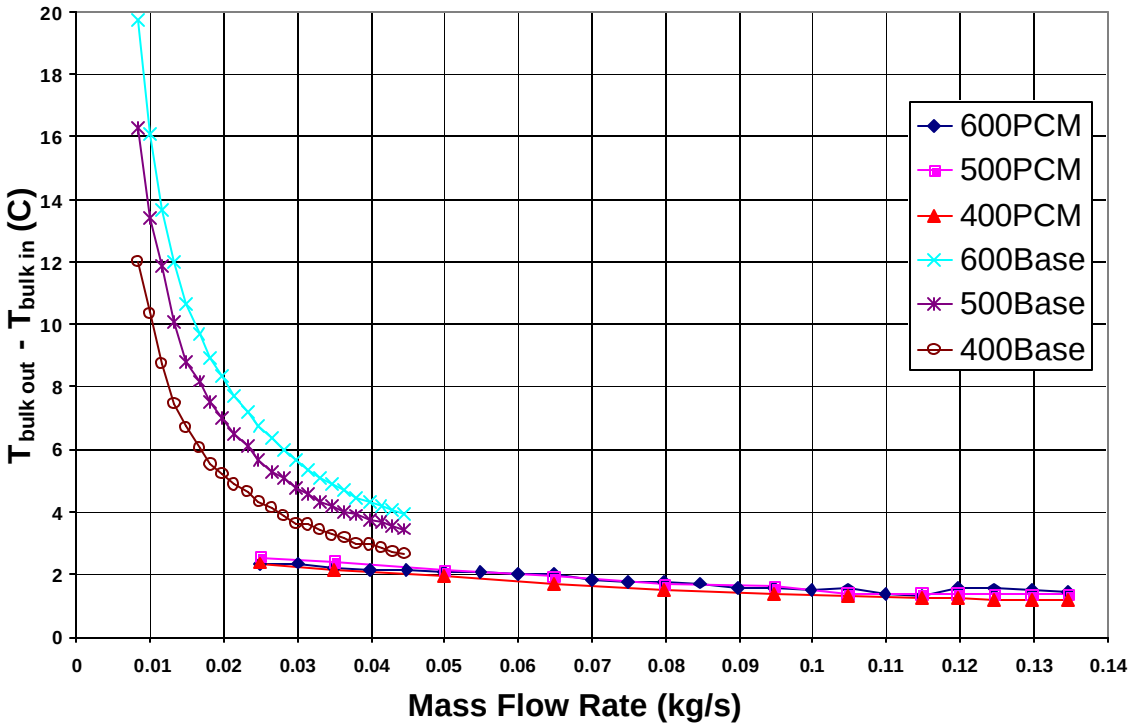

Figure18: Bulk fluid temperature change across heat section versus mass flow rate

Equally important, a constant bulk fluid temperature increase across the heat source for different heat rates at the same flow rate, suggests that in each of the three cases, the microPCM fluid has un-melted PCM particles at the exit of the heat section. Because there are still PCM particles to absorb latent heat, the bulk fluid temperature differential for the microPCM fluid remains nearly constant, regardless of heat input, over all flow rates tested. This should be the case as long as the applied heat energy and flow rate are such that there are still some solid, un-melted, octacosane particles remaining at the exit of the tube. In these steady-state tests, there was never enough heat energy applied, nor was the microPCM fluid pumped slowly enough, to melt all the PCM particles. Conversely, in figure 18, it is apparent that for the baseline fluid, a decrease in fluid flow rate yields considerably larger required temperature increases across the heated section.

Figure 19 shows the bulk fluid temperature difference across the heated section versus pressure drop across the heated section multiplied by mass flow rate. The pressure transducers intended to measure pressure drop across the heated section worked poorly, becoming clogged with PCM particles. Instead, a differential water manometer was used to verify analytically calculated pressure drops. Using the Hagen-Poiseuille theory[26] of internal flow through a pipe with constant cross section, the governing Navier-Stokes differential equation in cylindrical form reduces to

$$m\left(\frac{d^2u}{dy^2}+\frac{1}{y}\frac{du}{dy}\right)=\frac{dp}{dx} \qquad (7.2\text{-}2)$$

Where u is the velocity component parallel to the x-axis and y denotes the radial coordinate from the centerline outward. The solution to 7.2-2 gives a parabolic shaped velocity distribution, u(y). Knowing this, laminar pressure drops with relation to mass flow rate, viscosity, density, and internal pipe diameter were calculated as follows in 7.2-3.

$$\frac{dp}{dx}=-\frac{8\dot{m}m}{prR^4} \qquad (7.2\text{-}3)$$

Results obtained using 7.2-3 compared well with manometer measurements taken from the pumped loop using the microPCM fluid as the working fluid. Table 6 shows three points for comparison.

Table 6: Experimental versus analytical pressure drop across heat section

m_{dot} (kg/s)	Analytical (in H_2O)	Experimental (in H_2O)
0.025	0.2335	0.23
0.040	0.3765	0.38
0.050	0.4722	0.48

The pump power is defined as

$$W_p = \frac{\dot{m}\Delta p}{r} \tag{7.2-4}$$

The x-axis of figures 19 and 20 is easily converted to pumping power, in watts or $\frac{kgm^2}{s^3}$, by dividing by the density of the working fluid, ?; the relation of the curves changes little, as the density of both fluids are similar.

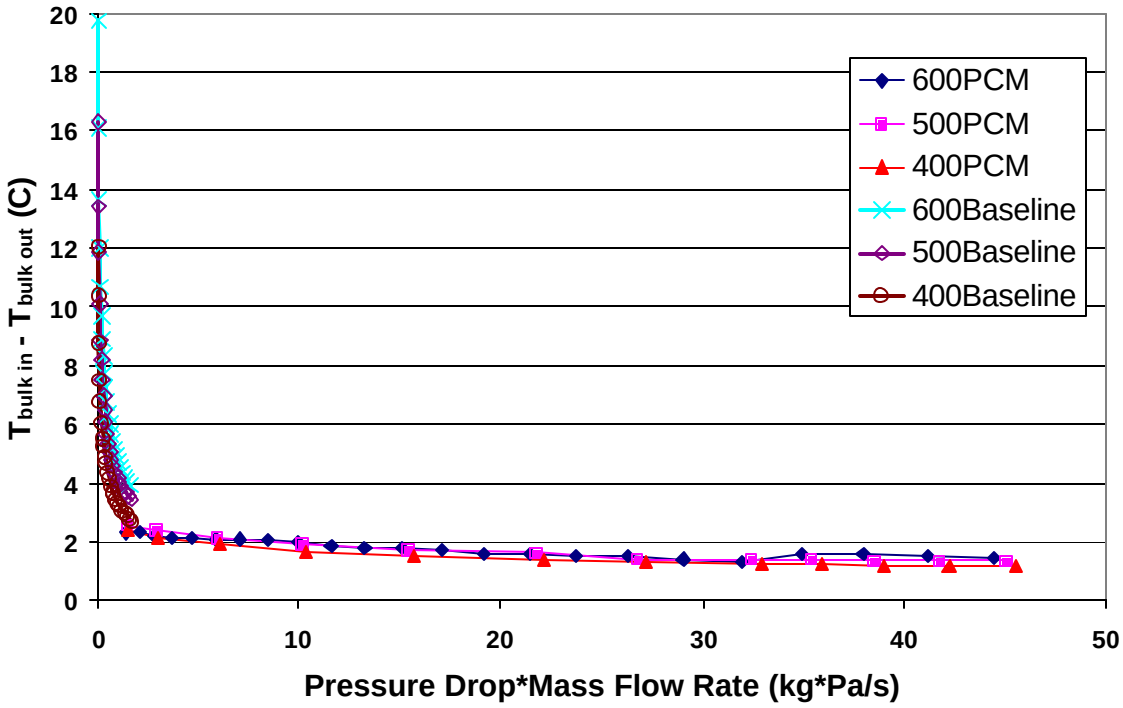

Figure 19: Bulk fluid temperature change across heated section versus pumping power

Since the microPCM fluid has approximately three and one half times the baseline fluid viscosity, it requires more pumping power to circulate. Figures 19 and 20 consider the pumping power when evaluating the heat transferred by the fluid; figure 20 is a low pumping power close-up of figure 19. These figures indicate that the microPCM fluid is most efficient when pumped slowly enough to allow the PCM particles enough residence time to change phase, but quickly enough that all of the PCM particles do not melt. At Q_{supply} = 600 watts and a mass flow rate of 0.0249 kg/s, data show that a good amount of PCM particles remain

un-melted. It is expected that the bulk fluid temperature increase across the heated section will follow the dotted curve shown in figure 20 for ultra low flow rates. However, the point where the temperature differential increases suddenly on the dotted curve was selected some what arbitrarily; that point depends on the amount of heat introduced to the heated section. If all of the PCM particles are melted before reaching the end of the heated section, the microPCM fluid should not perform as well as the baseline fluid.

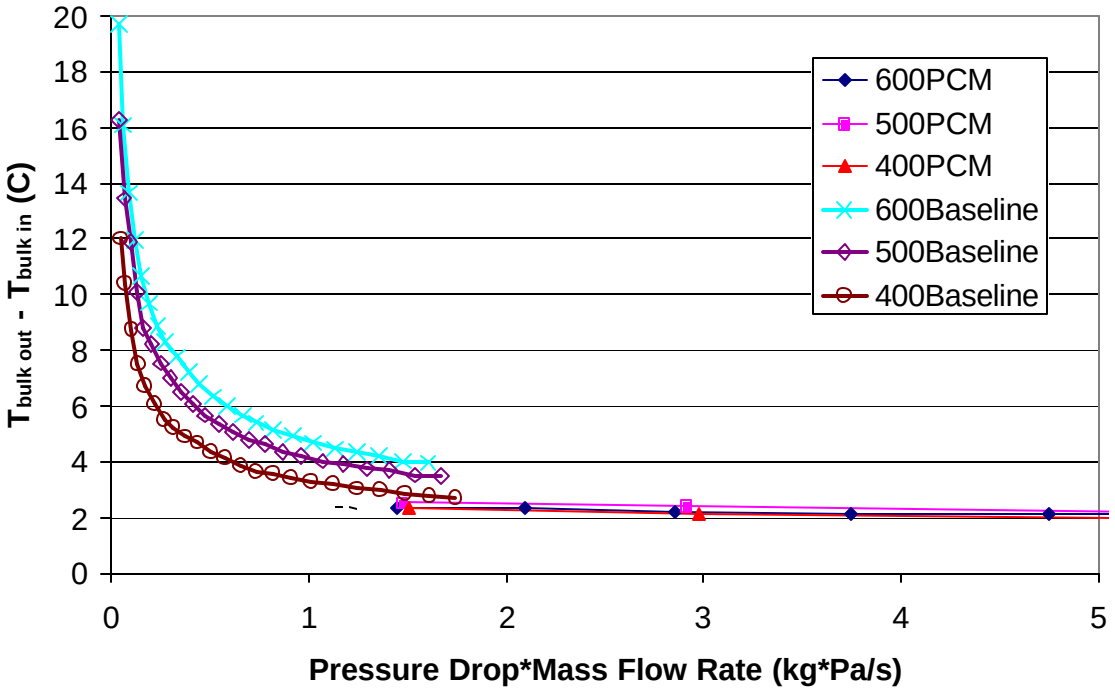

Figure 20: Bulk fluid temperature change across heated section versus pumping power

Figure 21 shows the mean fluid temperature increase across the heated section versus the specific heat energy input, $Q/\dot{m}$. This curve will be linear for sensible fluids; the bulk fluid temperature increase across the heated section is directly proportional to the amount of heat energy a given mass of sensible fluid absorbs. Indeed, figure 21 shows the baseline fluid has a linear relation between bulk fluid temperature increase and specific energy input. A latent fluid is expected to have a lower and more constant bulk fluid temperature increase

across the heated section. Since octacosane material changes phase nearly isothermally and large amounts of energy are absorbed during that phase change, the fluid temperature increase does not directly reflect the amount of heat energy a given mass of fluid absorbs. The microPCM curves are almost flat, indicating latent heat absorption.

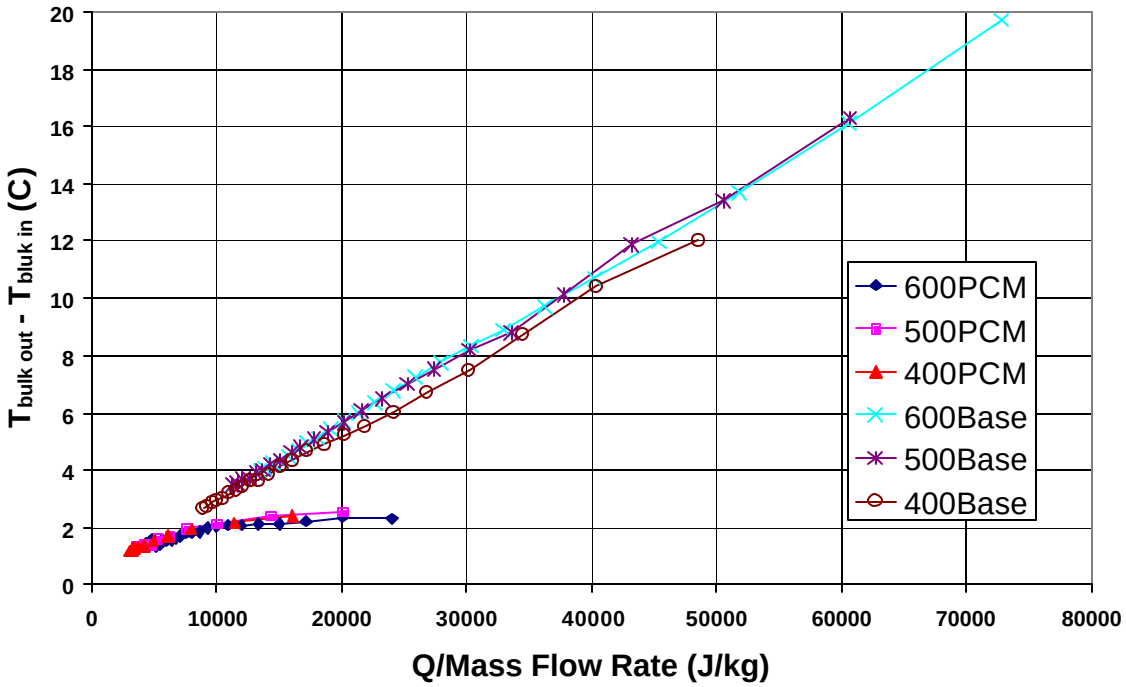

Figure 21: Bulk fluid temperature change across heated section versus specific energy input

Figure 22 shows the mean fluid temperature increase across the heated section versus Reynolds number. To calculate Re_D, equation 6.1-2 is used. This dimensionless parameter standardizes fluid flow and shows the point where turbulent transition takes place. The Reynolds number is varied by changing the mass flow rate in figure 22. The plot again shows us that the temperature increase across the heated section is about the same for the microPCM fluid, regardless of heat input. When the viscosities of the two fluids are considered, as is the case when Re_D is used, the microPCM yields drastic reductions in the

required bulk fluid temperature differential. This trend continues for both laminar and turbulent Re_D.

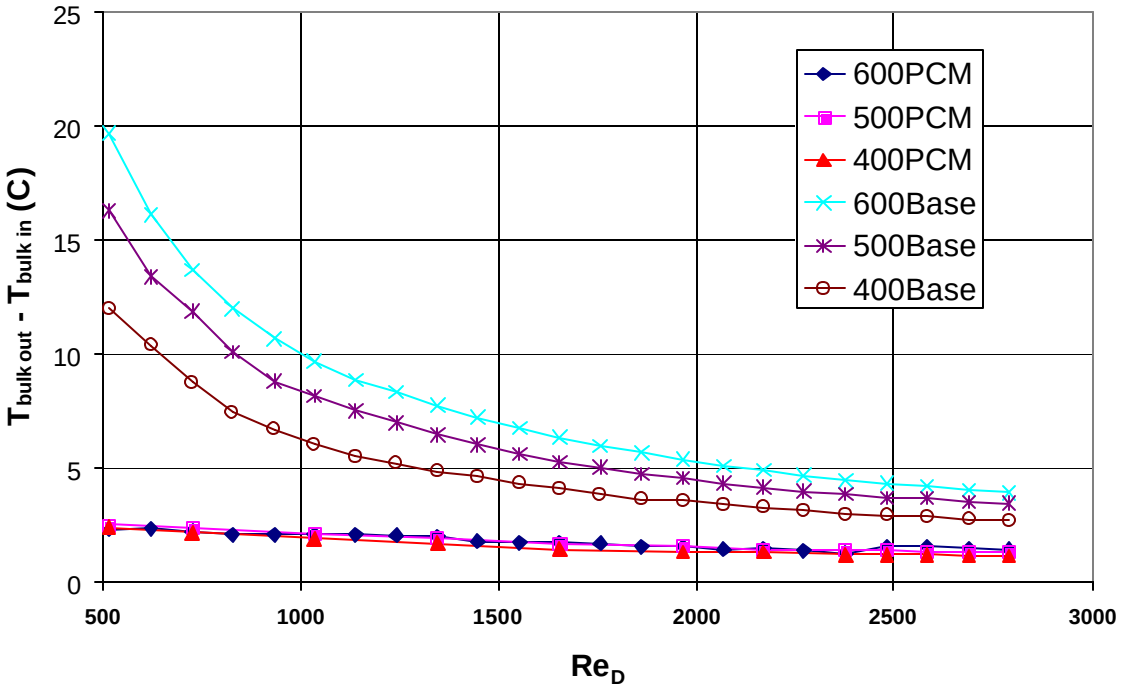

Figure 22: Bulk fluid temperature change across heated section versus Re_D

7.2.3 Exit Surface Temperature

This section compares exit surface temperature, T_{s-8}, referenced to inlet temperature, $T_{bulk\ in}$, versus the same parameters used in section 7.2.2. Figure 23 shows that, for a 0.01384 meter inner diameter copper tube heated section; the microPCM fluid provides lower exit surface temperatures than the 50/50 baseline solution at mass flow rates below 0.035 kg/s. This critical flow rate is nearly the same, regardless of the applied heat rate, so long as un-melted PCM particles remain at the exit of the heat section tube. The viscosity of the baseline fluid is much lower than the microPCM fluid, thus transition to turbulent flow occurs at much lower mass flow rates. When the baseline fluid flow becomes turbulent, the

convection heat transfer coefficient is augmented and the exit wall surface temperature drops below that of the microPCM fluid, which is still in the laminar flow regime at this mass flow rate.

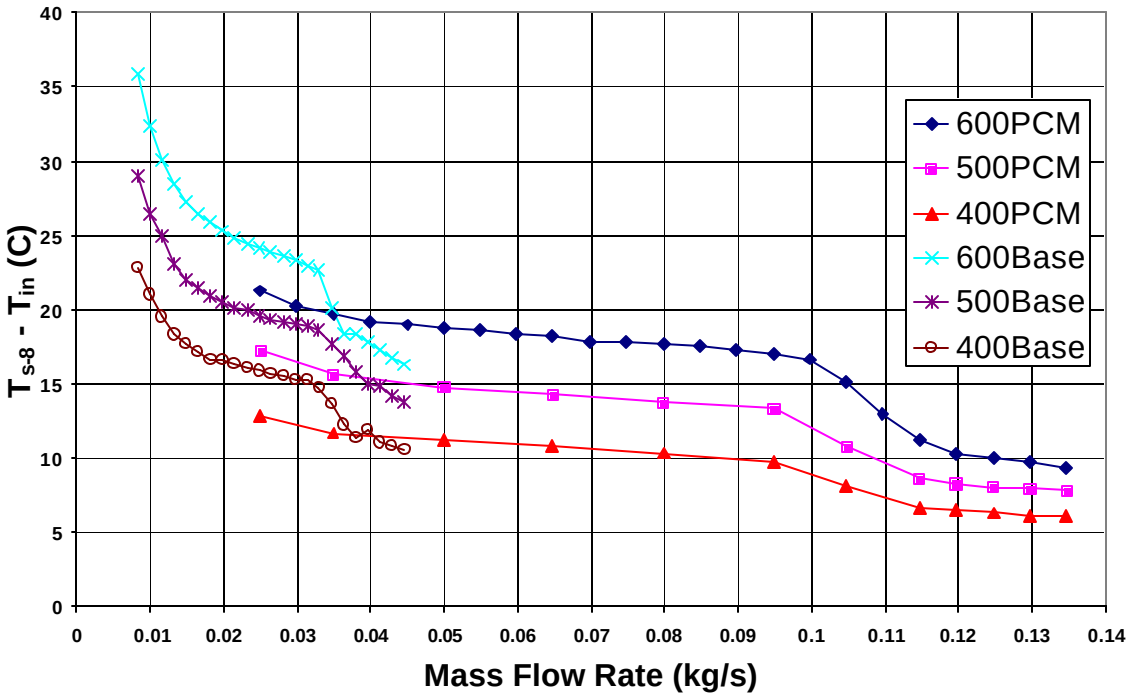

Figure 23: T_{s-8}, exit surface temperature, minus $T_{bulk\ in}$ versus mass flow rate

Figure 24 considers exit surface temperature, referenced to $T_{bulk\ in}$ versus pressure drop times the mass flow rate. Figure 25 is a low pumping power close-up of figure 24. Figure 25 illustrates the low viscosity of the baseline fluid by the small pumping power required to transition to turbulent flow. For the heat rates and flow rates considered with 23 percent PCM particle concentration in the microPCM fluid, the performance of the PCM is no better than the baseline when pumping power is considered. However, experimental results show the microPCM fluid is not operating at peak efficiency because there are PCM particles that are not melting across the heated section, but the dynamic viscosity of the microPCM is about 3.5 times that of the baseline fluid. Unfortunately, a case was not run

where all the microPCM particles were melted across the heated section. However, when Q_{supply} = 600 watts at the lowest mass flow rate run for the microPCM fluid, 0.0249 kg/s, there is still un-melted PCM particles exiting the heated section. This means there must be at least enough un-melted PCM particles at the exit when Q_{supply} = 400 watts at the same mass flow rate of, 0.0249 kg/s, to absorb 200 plus watts of heat energy.

A simple calculation should give a rough idea of the mass flow rate that will allow all PCM particles to melt across the heated source when Q_{supply} = 600 watts. From the differential scanning calorimeter data we know that the microPCM fluid has a heat of fusion of 49.4 J/g. From the dimensions of the heated section tube, the volume of fluid in the heat section tube able to absorb heat at one time is

$$V_{hs} = l \times A_c = 1.804m \times \left(0.0069215^2 p\right) = 0.0002714m^3 \tag{7.2-5}$$

Using the density of the 23 percent microPCM fluid, the mass of fluid in the heated section is

$$Mass_{PCM-hs} = V_{hs} \times r_{PCM} = 0.0002714m^3 \times 1020kg/m^3 = 0.2768kg \tag{7.2-6}$$

So using the heat of fusion, the energy storage capacity for the fluid in the heat section, independent of flow rate, is

$$E_{PCM-hs} = 0.2768\,kg \times 49400\ J/kg = 13{,}674\,J \tag{7.2-7}$$

Now the residence time of the fluid in the heat section must also be considered so

$$t_r = Mass_{PCM} / \dot{m} \tag{7.2-8}$$

For a mass flow rate of 0.0122 kg/s, the residence time is 22.8 seconds. Since

$$Q_{act} = E_{PCM-hs} / t_r \tag{7.2-9}$$

At 600 watts, a residence time of 22.8 seconds should just melt all the PCM particles in the heated section tube. At that residence time, the pressure drop $\times$ mass flow rate is less than 0.5 kg^2/s^3-m, and though no experimental tests were run at these low flow conditions, trends indicate the fluid temperature increase across the heated section and the surface temperatures would be less when compared to the baseline under the same heat and flow conditions.

Just as the microPCM fluid was not pumped slowly enough to melt all of the PCM particles, the quantity of pumping power required to produce turbulent flowing microPCM fluid was not applied to the baseline fluid. However, included in figure 24 is a correlation from a text by Incropera and DeWitt[27] submitted by Gnielinski, that gives a Nusselt number correlation for flow through smooth tubes. The correlation is valid for Prandtl numbers between 0.5 and 2,000 and Re_D between 3,000 and 5,000,000. This correlation is valid for uniform surface heat flux and surface temperature; it is presented as equation 7.2-10.

$$Nu_D = \frac{(f/8)(Re_D - 1000)Pr}{1 + 12.7(f/8)^{1/2}(Pr^{2/3} - 1)} \qquad (7.2\text{-}10)$$

The Re_D is presented in equation 6.1-2, the Prandtl number is tabulated, and the friction factor for flow in smooth tubes is defined by

$$f = (0.790 \ln Re_D - 1.64)^{-2} \qquad (7.2\text{-}11)$$

As is the case of many correlations that are applied to transitional turbulent flow, the convection coefficient may be slightly over predicted; this would predict lower surface temperatures than actual. However, this correlation appears to fit the data well. It indicates that the pumping power required to cause turbulent flow in the microPCM fluid may be better spent on the baseline fluid when surface temperature is concerned. Modest 10 percent error bars are included with the correlation curve.

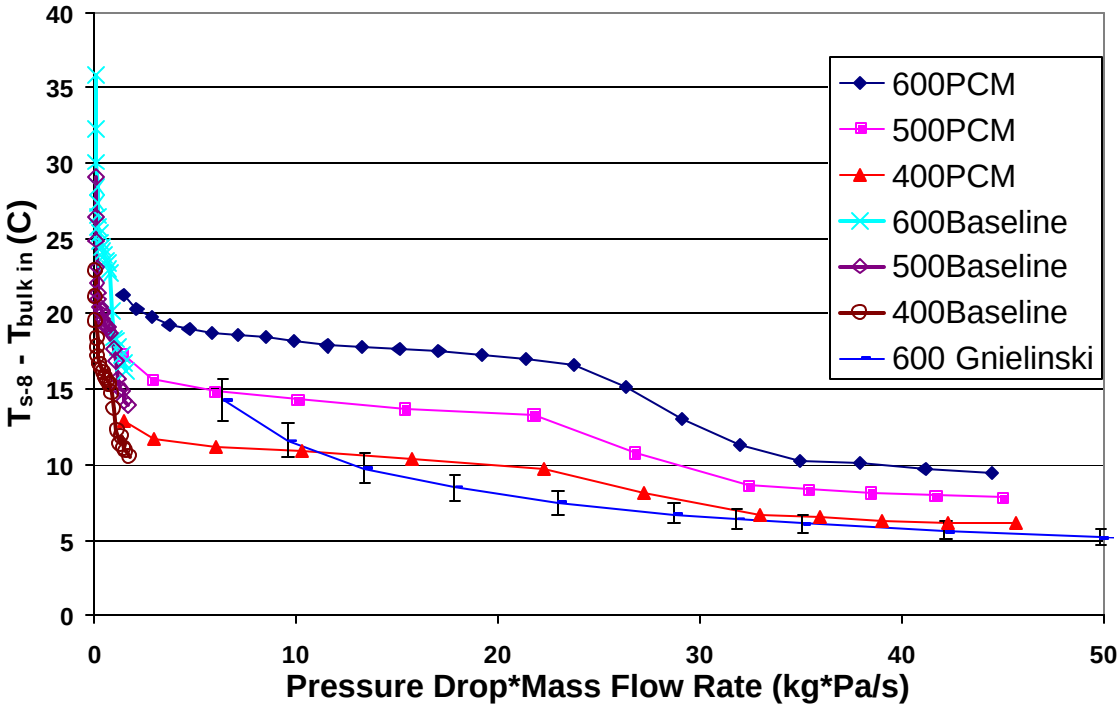

Figure 24: T_{s-8}, exit surface temperature, minus $T_{bulk\ in}$ versus flow rate × pressure drop

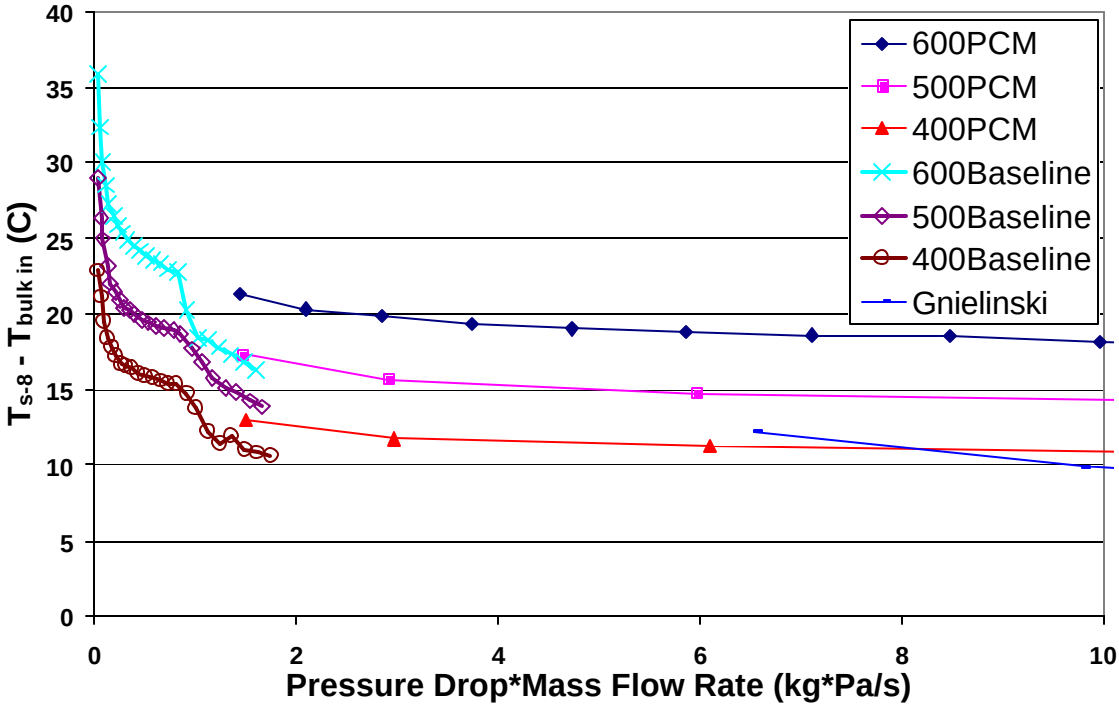

Figure 25: T_{s-8}, exit surface temperature, minus $T_{bulk\ in}$ versus mass flow rate × pressure drop

Figure 26 gives the referenced exit surface temperature versus specific heat energy input into the fluid. It reveals, as expected, that the microPCM fluid provides lower surface temperatures than the baseline fluid at high specific energy input. As discussed previously, this trend will continue until the specific energy becomes greater than the amount the PCM can absorb, somewhere around 50,000 J/kg. Up until this point, the more heat the PCM can absorb, the more efficient the microPCM fluid becomes.

Figure 27 shows the referenced exit surface temperature over the Reynolds numbers tested. When the Reynolds number is used as the independent parameter, the microPCM fluid shows noteworthy reduction in wall surface temperature over all Re_D, laminar and turbulent. However, because of viscosity, larger mass flow rates are required for the microPCM fluid to have the same Re_D as the baseline fluid. The most significant surface temperature reductions occur at low Re_D, thus, low mass flow rates; this is where the microPCM fluid is most effective.

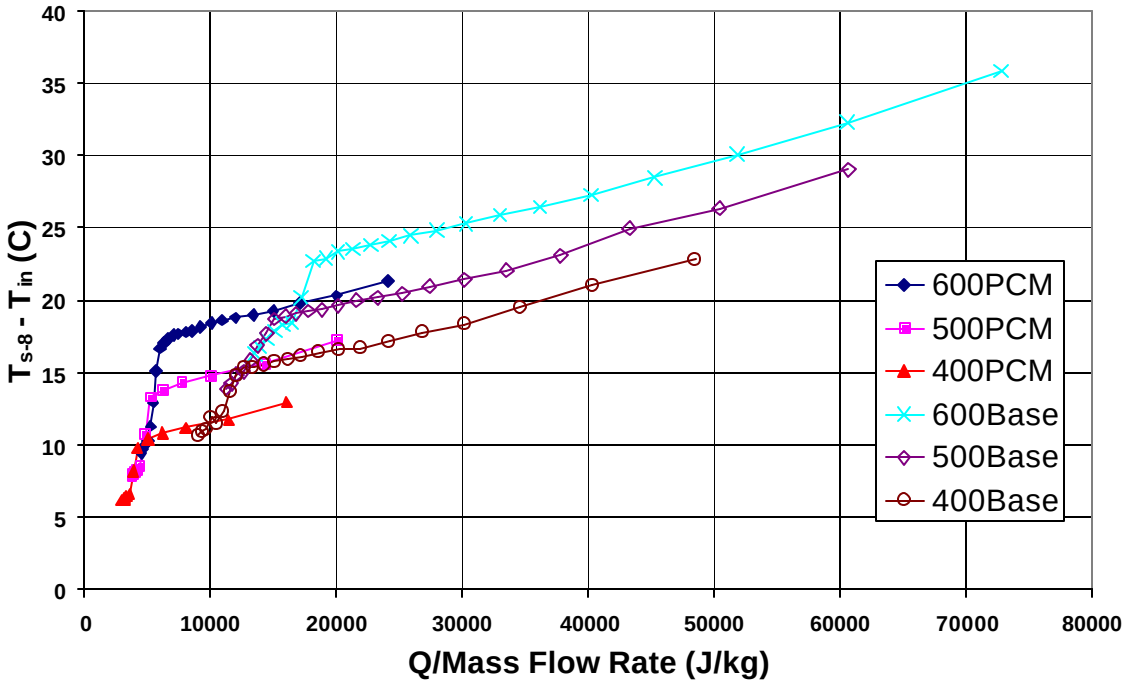

Figure 26: T_{s-8}, exit surface temperature, minus $T_{bulk\ in}$ versus specific energy input

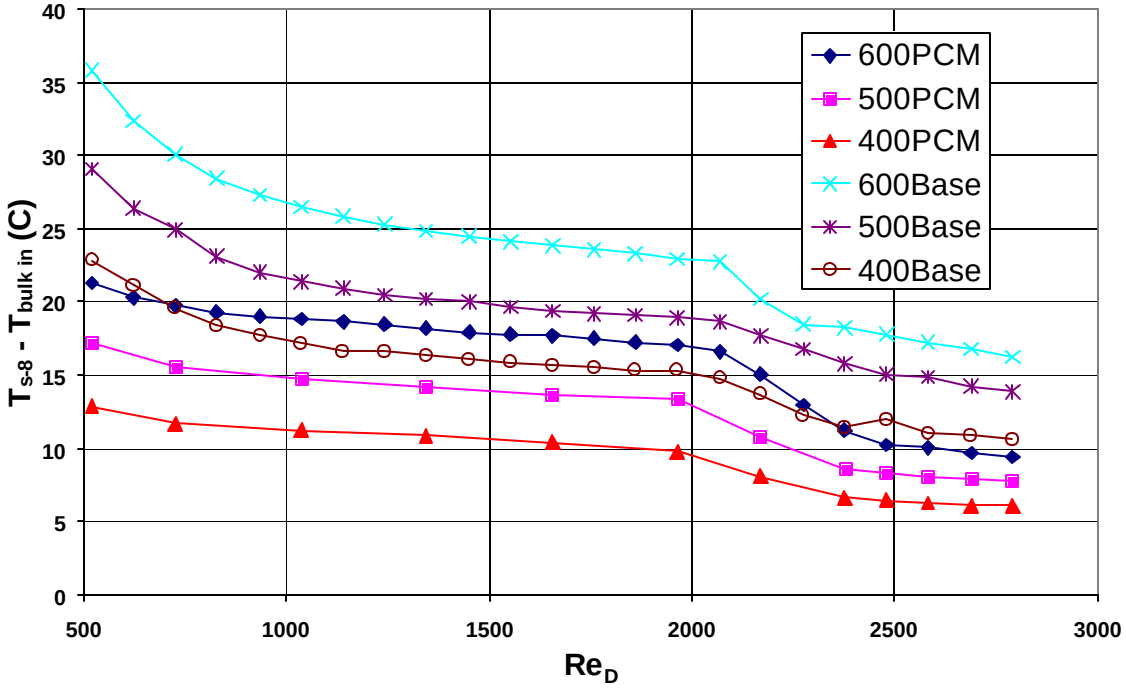

Figure 27: T_{s-8}, exit surface temperature, minus $T_{bulk\ in}$ versus Re_D

7.3 Transient Input Temperature Results

As described in the flow parameters section, this test compares the microPCM fluid with the baseline solution at one specific mass flow rate, but at multiple bulk mean fluid inlet temperatures, $T_{bulk\ in}$. The mass flow rate is determined by choosing equal Re_D for the two fluids when $T_{bulk\ in}$ = 60°C. This test data compares well with the steady-state data, so we could consider this transient experiment quasi-steady-state. In figure 28, when $T_{bulk\ in}$ = 60°C, Re_D = 933 for both fluids and Q_{supply} = 600 watts. We can see that the microPCM fluid still posses the properties of a sensible fluid when the PCM particles are not undergoing a phase change. This is seen when, $T_{bulk\ in}$, the bulk mean inlet temperature on the x-axis, is less than 40°C or greater than 62°C. In these two cases there is little or no latent heat absorption by the PCM particles; all heat energy absorbed by the microPCM fluid is sensible. The

microPCM fluid might perform slightly worse than the baseline fluid once all the PCM has melted. This is expected since the volume of PCM particles, which can no longer absorb latent heat, limit the volume of sensible carrier fluid. The transient data supports this, but when the microPCM fluid is operating under design conditions, these single-phase inlet temperatures will not be reached. When the microPCM fluid operates under tuned conditions, the data reveals an impressive decrease in wall surface temperature of 6°C to 7°C at the heated tube exit. This data also shows a much smaller bulk fluid temperature increase across the heated section when the octacosane changes phase. The transient data was very similar for all laminar Reynolds numbers. The same trends continue for turbulent flow, however, the slope of the curves changed.

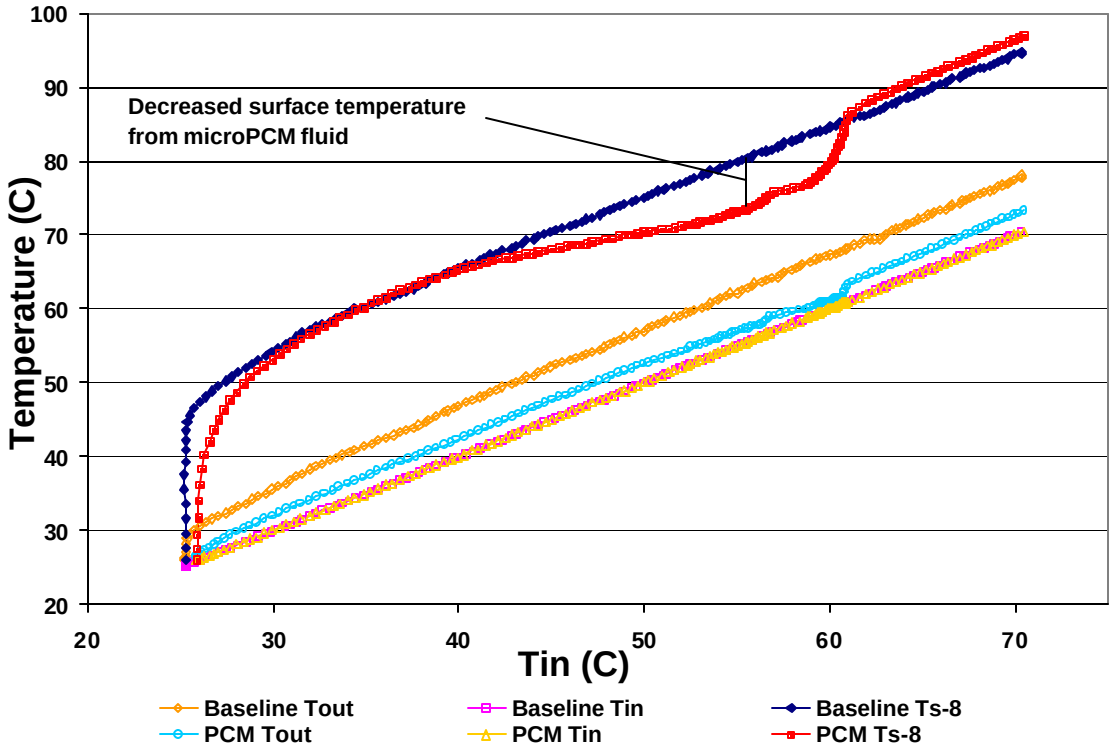

Figure 28: $T_{bulk\ in}$ versus selected temp readings, Re_D=933 at $T_{bulk\ in}$=60°C , Q_{supply}=600 watts

Figure 29 is a close-up of the fluid temperature increase that the 23% octacosane microPCM fluid experiences across the heated section versus different inlet temperatures. This data was taken when Q_{supply}=600 watts and mass flow rate is 0.0455 kg/s. This data is similar to the data presented in the differential scanning calorimeter section because the heat absorbed by the phase change is apparent. Figure 29 shows that when $T_{bulk\ in}$ is in-between 50.0°C and 57.0°C, the octacosane PCM undergoes a solid to solid phase change. The PCM undergoes a solid to liquid phase change from 57.0°C until all particles have liquefied at 61.2°C. The greatest amount of latent heat is absorbed in the solid to liquid phase change and it is recommend the microPCM fluid be run at that condition for optimum performance. This plot also shows that a small bulk fluid temperature differential of only 1°C is required to transfer the 600 watts of heat energy when the microPCM fluid undergoes phase change; a delta T of 2°C to 3°C is required when there is no change in phase of the microPCM fluid.

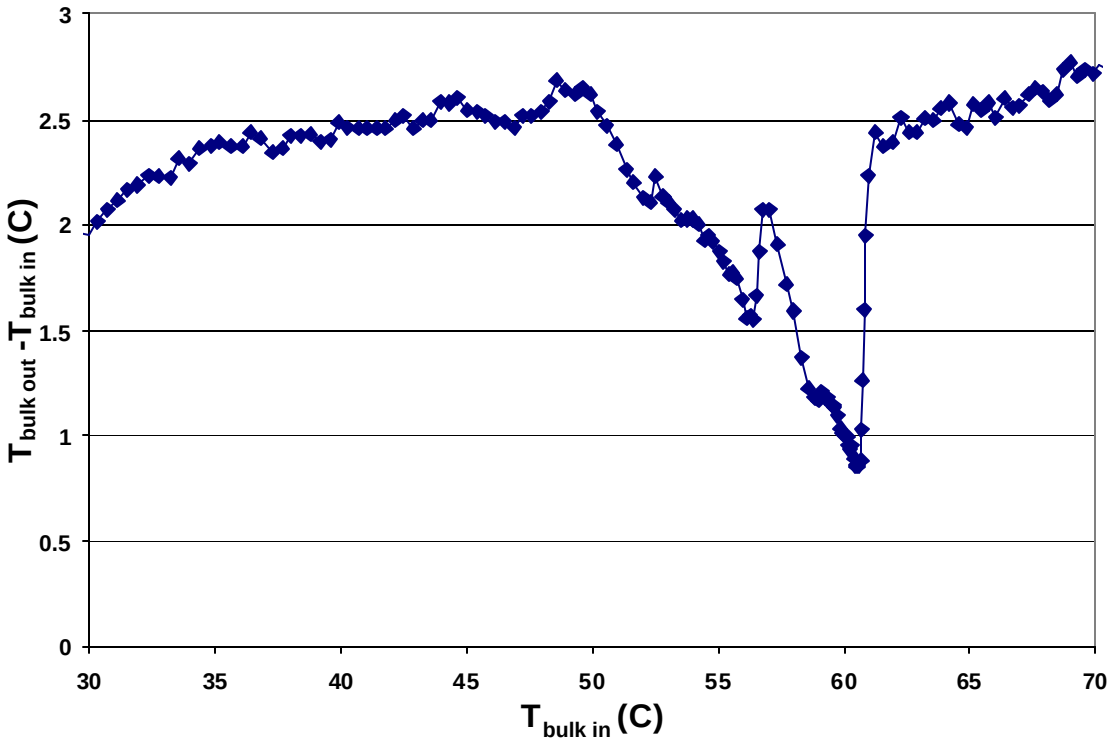

Figure 29: Fluid temperature across heat section versus $T_{bulk\ in}$, Q_{supply}=600 watts, mass flow rate = 0.0455kg/s, Re_D=933 when $T_{bulk\ in}$=60°C

7.4 Calculated Results

Derived heat transfer parameters were obtained from the experimental steady-state results. An average and local heat transfer convection coefficient are presented. Finally, the effective specific heat for the microPCM fluid is presented.

7.4.1 Heat Transfer Convection Coefficient

Figure 30 depicts the length averaged convection heat transfer coefficient, h_m, of the baseline and the microPCM fluid over a range of laminar and turbulent flow conditions. The average convection coefficient was estimated using equation 7.4-1.

$$h_m = Q_{act} \Big/ \left(\overline{T_s} - \overline{T_b}\right) \tag{7.4-1}$$

$\overline{T_s}$ is the average of the eight wall surface temperatures, Ts-1 through Ts-8, and $\overline{T_b}$ is the average of the inlet, $T_{bulk\ in}$, and outlet, $T_{bulk\ out}$, bulk mean fluid temperatures. This simple approach agrees well with the formal definition,

$$h_m = 1 \Big/ L \int_0^L Q_{act} / \left(T_s(x) - T_b(x)\right) dx \tag{7.4-2}$$

where $T_s(x)$ and $T_b(x)$ are curve fit to the experimental data and h_m is determined analytically.

The laminar microPCM data shows an increase of 20% in h_m when compared to the ethylene-glycol/water baseline solution. In the transitional turbulent flow region, mixing from the solid particles increases the enhancement of h_m for the microPCM fluid to approximately 30% over the baseline fluid.

To verify the data in figure 30, two correlations for single phase fluids are included. The Leveque correlation, from Eckert and Drake[28], for laminar thermal entry heat transfer problems gives the length mean Nusselt number, a dimensionless temperature gradient at the wall surface, as 7.4-3.

$$Nu_m = 1.76 Gz_L^{0.333} \tag{7.4-3}$$

Knowing the Graetz number is given as

$$Gz_x = \frac{\mathrm{Re}_D \,\mathrm{Pr}}{(x/D)} \tag{7.4-4}$$

For the heated section of the flow loop, L/D = 114.5, the Nusselt number correlation becomes

$$Nu_m = h_m D/k = 0.363 \mathrm{Re}_D^{0.333} \,\mathrm{Pr}^{0.333} \tag{7.4-5}$$

Experimental data from the baseline fluid matches this correlation when Pr = 20 and k = 0.456 W/m-°C. In figure 30, for low Re_D it is likely that, towards the exit of the tube, some viscous breakdown occurs in the baseline fluid, causing turbulent boundary layer flow. That is the reason h_m for the baseline fluid does not have the same slope as the PCM fluid at low Re_D.

The data of Sherwood et. al[29] presented in Sieder-Tate[30] for transitional turbulent flow in a circular tube between Re_D of 2300 and 4000 was fit to a correlation by Dalle Donne and Bowditch[31]. They determined an exponent of unity for Re_D based on a linear interpolation between laminar (Re_D = 2100) and fully turbulent (Re_D = 10,000) data. The correlation is

$$Nu_m = 0.0022 \mathrm{Re}_D \,\mathrm{Pr}^{0.333} \tag{7.4-6}$$

Figure 30 shows experimental data for the ethylene-glycol/water baseline agrees well with correlation 7.4-6 for transitional turbulent flow. The transition to turbulent flow results in a change of slope with Re_D.

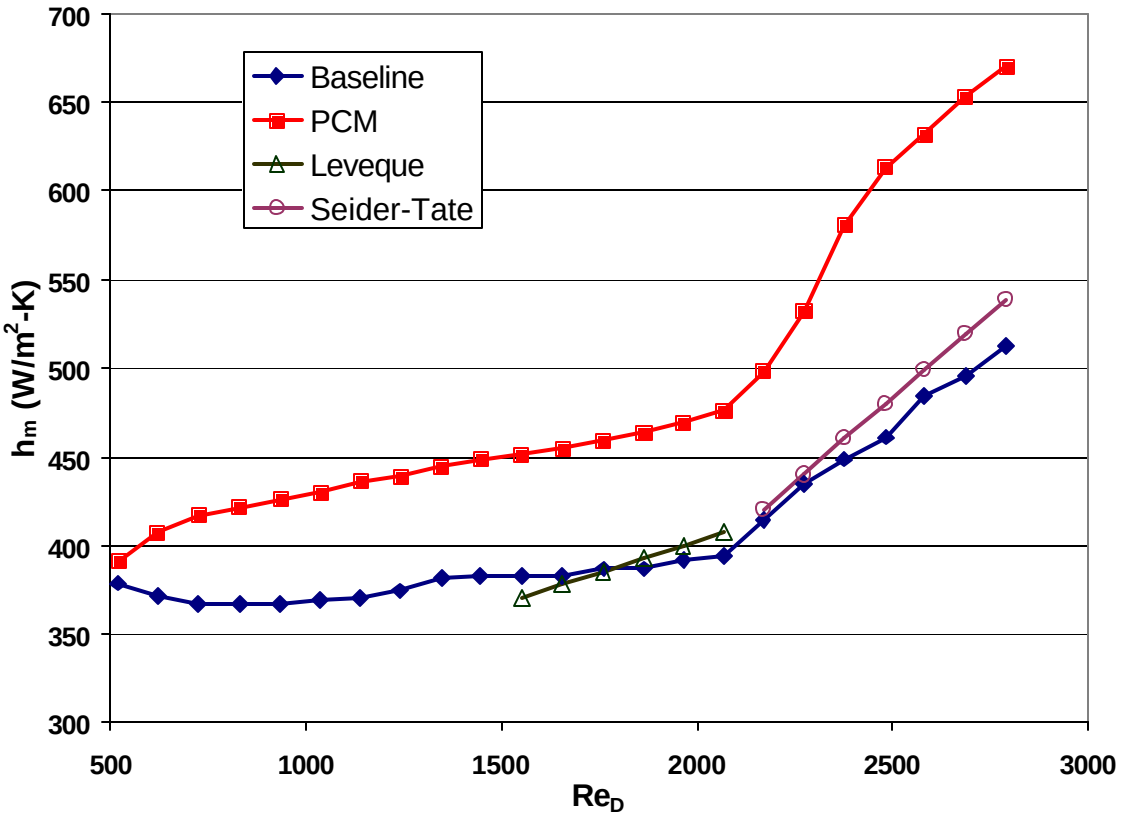

Figure 30: Length averaged convection coefficient versus Re_D

Figure 31 shows a local heat transfer convection coefficient, h_x. This convection coefficient is calculated at the entrance of the heat section when x = 0.062 meters from the tube entrance. For this local convection coefficient, ?T is found from subtracting T_{s-1}, the wall surface temperature at x = 0.062 meters, from the entrance fluid temperature, $T_{bulk\ in}$. This equation is given in equation 7.4-4.

$$h_{x=0.062} = Q_{act} / (T_{s-1} - T_{bulk-in}) \qquad (7.4\text{-}7)$$

At the heated tube entrance, the local convection coefficient for microPCM fluid performs at least 30 percent better than the baseline fluid. Under turbulent flow conditions, the microPCM continues to enhance the local entrance convection coefficient over the baseline fluid local entrance convection coefficient.

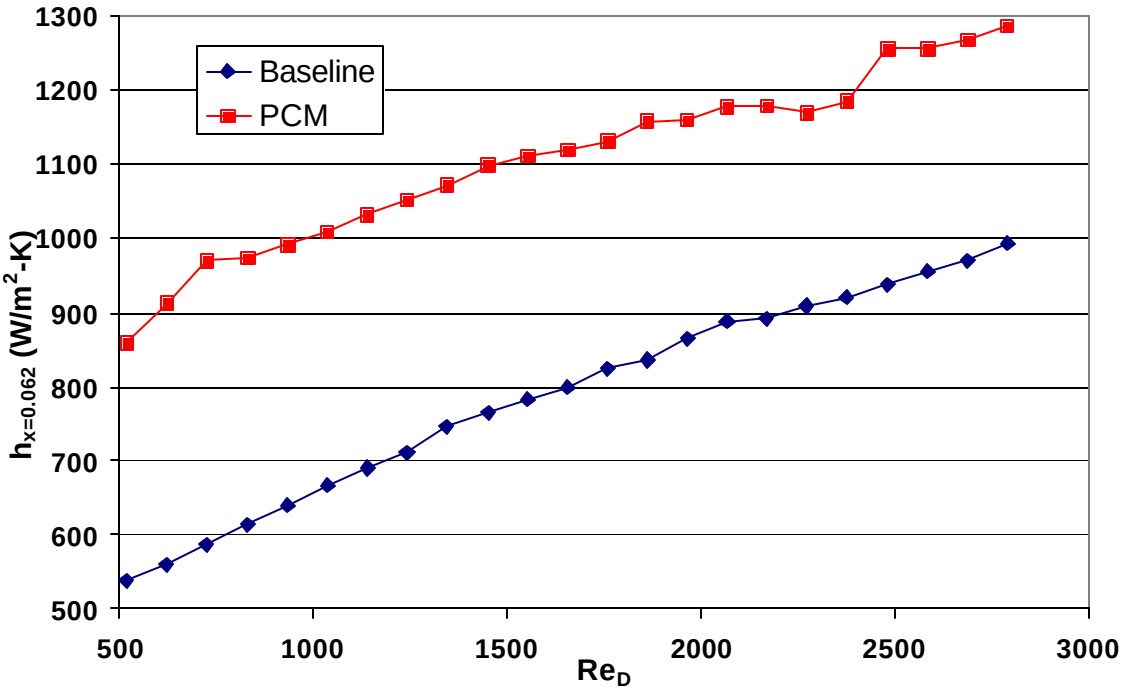

Figure 31: Local convection coefficient at tube entrance, x = 0.062 meters, versus Re_D

The local convection coefficient at x = 1.022 meters is presented in figure 32. The value of $h_{x=1.022}$ is found using the wall surface temperature at x = 1.022 meters, T_{s-5}. Since this local heat transfer convection coefficient is approximately in the middle of the heated section, the bulk fluid temperature is defined as the midpoint temperature of the fluid in the tube, $T_{mid} = (T_{bulk\ in} + T_{bulk\ out})/2$. Thus equation 7.4-8 gives the local convection coefficient at the heated tube midpoint.

$$h_{x=1.022} = Q_{act} / (T_{s-5} - T_{mid}) \qquad (7.4\text{-}8)$$

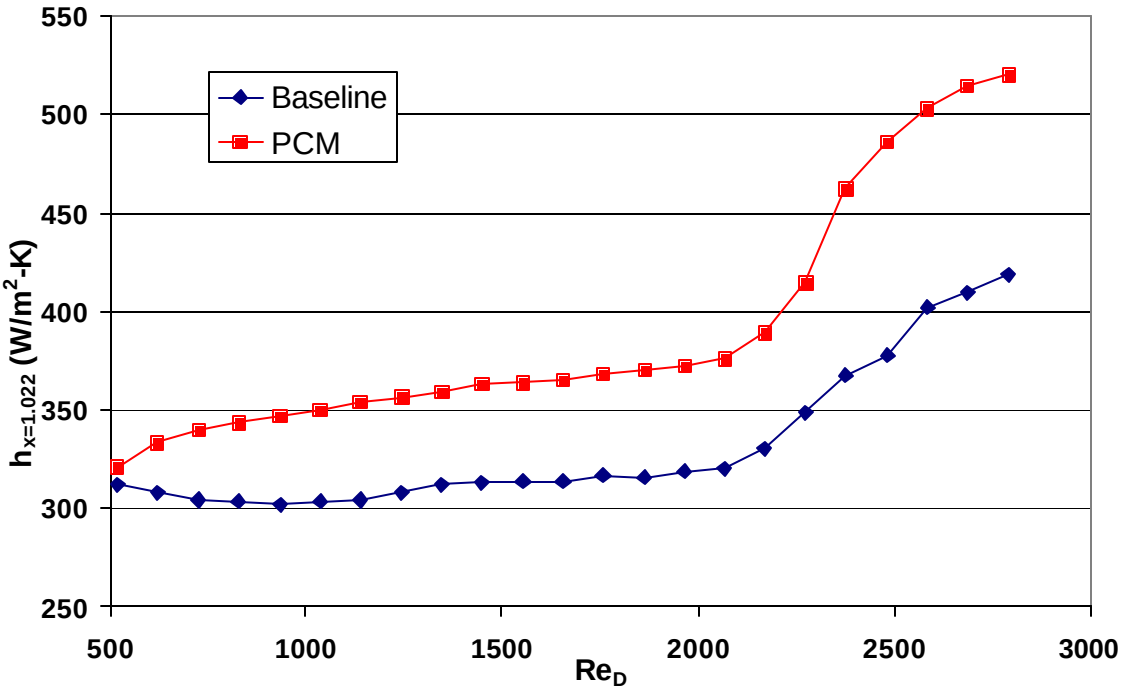

Figure 32: Local convection coefficient at x = 1.022 meters versus Re_D

The local heat transfer convection coefficient at the tube exit, x = 1.742 meters, is presented in figure 33. For this local convection coefficient, ? T is found from subtracting T_{s-8}, the wall surface temperature at x = 1.742 meters, from the bulk fluid exit temperature, $T_{bulk\ out}$. This equation is given in equation 7.4-9.

$$h_{x=1.742} = Q_{act} / (T_{s-8} - T_{bulk-out}) \qquad (7.4\text{-}9)$$

It is theorized that the dramatic enhancement of h_x at the tube exit, especially for turbulent flow, is caused by the solid particles in the fluid. The relative motion of the particles against the fluid creates microconvective effects which manifest itself in a form of eddy conductivity. Collingham[32] preformed an experimental investigation of mass transfer in flowing suspensions of polystyrene beads in aqueous sodium chloride. His results showed substantial increases in mass transfer for both laminar and turbulent flow. Kasza and Chen[19] conducted analytical studies of heat transfer in suspensions that suggested considerable

enhancement of the heat transfer convection coefficient due to microscopic solid particles suspended in the fluid. Figure 33 also indicates that the solid particles in the carrier fluid may prohibit the microPCM fluid from transitioning to turbulent flow when compared to the baseline fluid, which has no solid particle concentration.

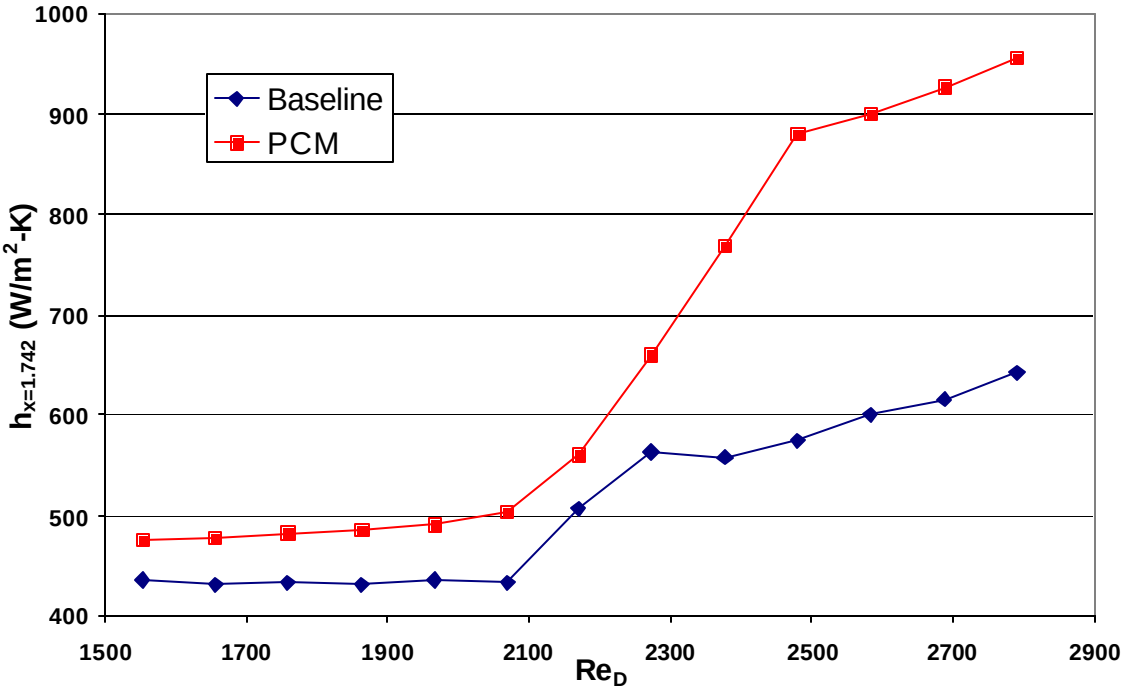

Figure 33: Local convection coefficient at the tube exit, x = 1.742 meters, versus Re_D

The heat energy used in the calculation of each convection coefficient was Q_{act}. Q_{act} is calculated by estimating the energy actually entering the fluid, as described at the beginning of the results section. That analysis gave a percentage of the heat energy supplied to the system, Q_{supply}, that actually enters the working fluid, Q_{act}. The remaining heat energy is lost to the environment. Using the system efficiency, calculated as 92.4 percent efficient, $Q_{act} = 0.924 \times Q_{supply}$.

7.4.2 Effective Specific Heat

The specific heat of the baseline ethylene-glycol/water solution was calculated by combining the published tabulated specific heats of the two constituents via their mass

fractions in the solution. These calculations follow procedures outlined for determining properties of solutions in the AIChE "Data Compilation Tables of Properties of Pure Compounds," the Department of Chemical Engineering, Penn State University[24]. The specific heat of the 50/50 baseline ethylene-glycol/water solution versus fluid temperature, along with the best fit curve equation used for calculations is presented in figure 34.

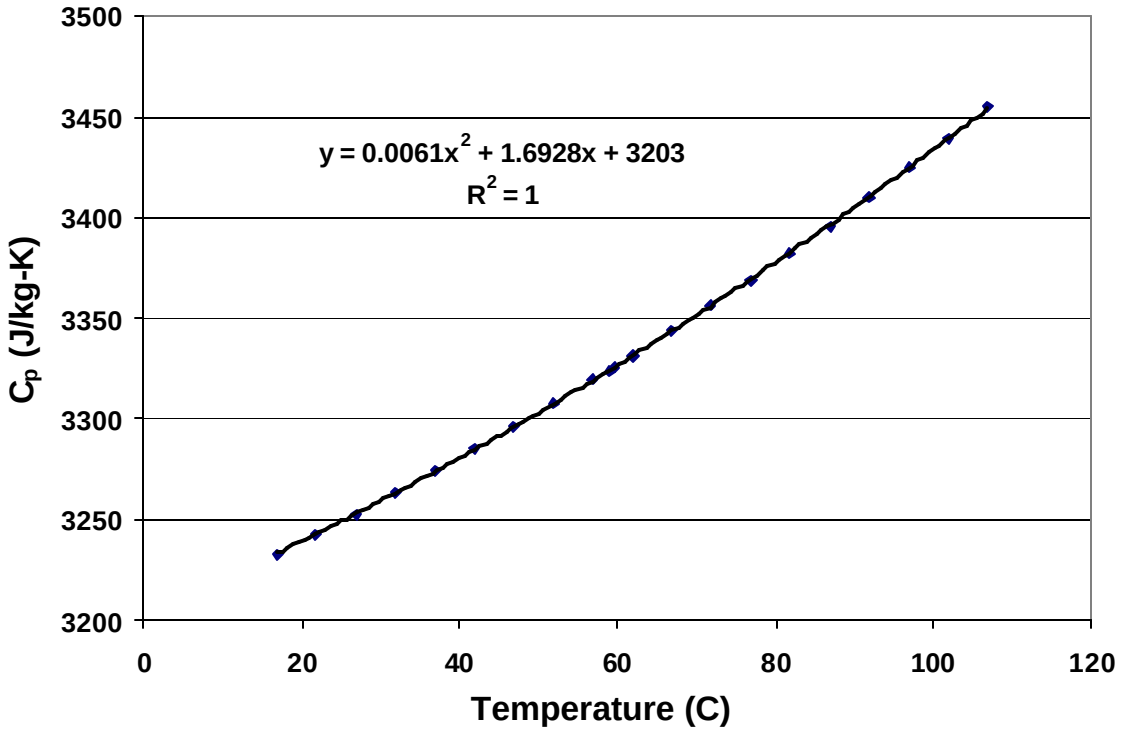

Figure 34: Tabulated specific heat versus temperature for 50/50 baseline fluid

The effective specific heat of the microPCM fluid was calculated using equation 7.4-10.

$$C_{p,eff} = \frac{Q_{act}}{\dot{m}(T_{bulk-out} - T_{bulk-in})} \qquad (7.4\text{-}10)$$

This equation accounts for latent and sensible energy absorbed by the microPCM fluid. Figure 35 illustrates specific heat and experimental effective specific heat of the baseline and the microPCM fluid, respectively, for Reynolds numbers less than 2900. Clearly, it is

advantageous to use the microPCM at low flow rates because of dramatic increases in effective specific heat. The data in figure 35 shows that effective specific heat of the microPCM fluid is dependent on resident time or, the amount of time the microPCM fluid is in the heated tube. The longer the microPCM fluid is in the heated tube, for a given heating power, the more latent heat the particles can absorb and carry away. The effective specific heat of the microPCM fluid should continue to increase with decreasing flow rate as long as un-melted octacosane particles remain in the microPCM fluid.

As expected, the specific heat of the baseline varies little with flow rate or residence time. In fact, the only variation in the baseline specific heat is from a change in fluid temperature. This fluid temperature difference comes from changes in wall surface temperature resulting from convection coefficients that are dependent on flow rate.

Notice the effective specific heat of the microPCM fluid drops below that of the baseline as Reynolds numbers enter the turbulent regime. With the short length of the pumped loop heated section tube, at turbulent flow rates the microPCM particles have little residence time to react to the applied heat. The microPCM fluid moves across the heated section so quickly, that the carrier fluid can not transmit the heat to the particles so that they might change phase. By combining the tabulated specific heats of the constituents in the microPCM fluid, using a mass fraction basis, the specific heat of un-reacted microPCM fluid, when no octacosane changes phase, is estimated at about 2730 J/kg-°C. This specific heat is around 17 percent less that the 50/50 ethylene-glycol/water baseline solution. The decrease in specific heat is attributed to the low specific heat of the microPCM particles, which constitute 23 percent of the microPCM fluid mass. Note that the microPCM particles will change phase in turbulent flow fine, they just have to have sufficient residence time in the heated section to absorb the

heat. Even at the small residence time associated with high Re_D in the heated tube, some particles are still changing phase.

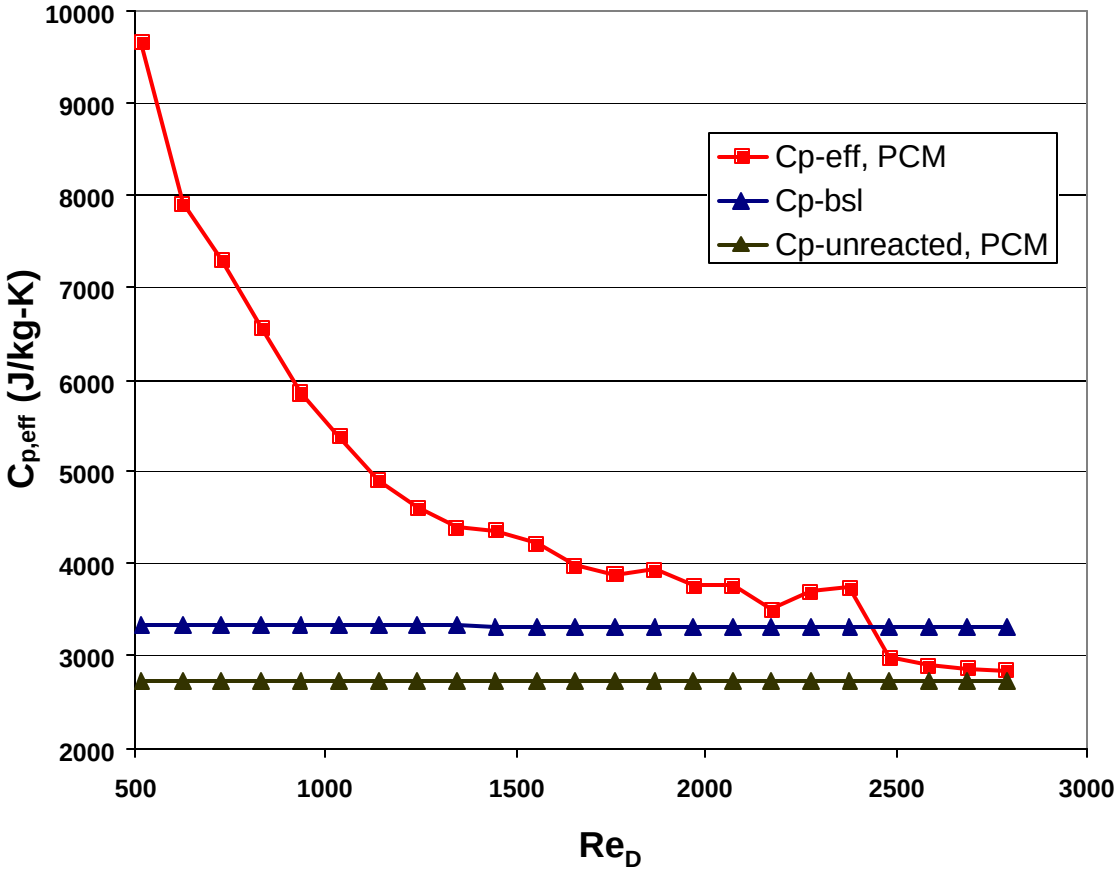

Figure 35: Effective specific heat versus Re_D

A ratio of effective specific heat is presented in figure 36. The ratio of microPCM fluid effective specific heat to baseline specific heat values presented in figure 35 yields the curve given in figure 36. Again, this plot indicates the effectiveness of the PCM fluid as a heat transfer fluid. The figure reveals a dependency between effectiveness and the flow rate, or residence time in the heat source, of the microPCM fluid. For a 2.08 meter tube, the largest increases in effective specific heat occur at flow rates that yield a Reynolds number less than one thousand. This is so because the PCM can absorb more latent heat energy when the flow is slow and the octacosane has sufficient resident time within the heat source section

to change phase. Low flow rates also decrease the pumping power required to circulate the fluid.

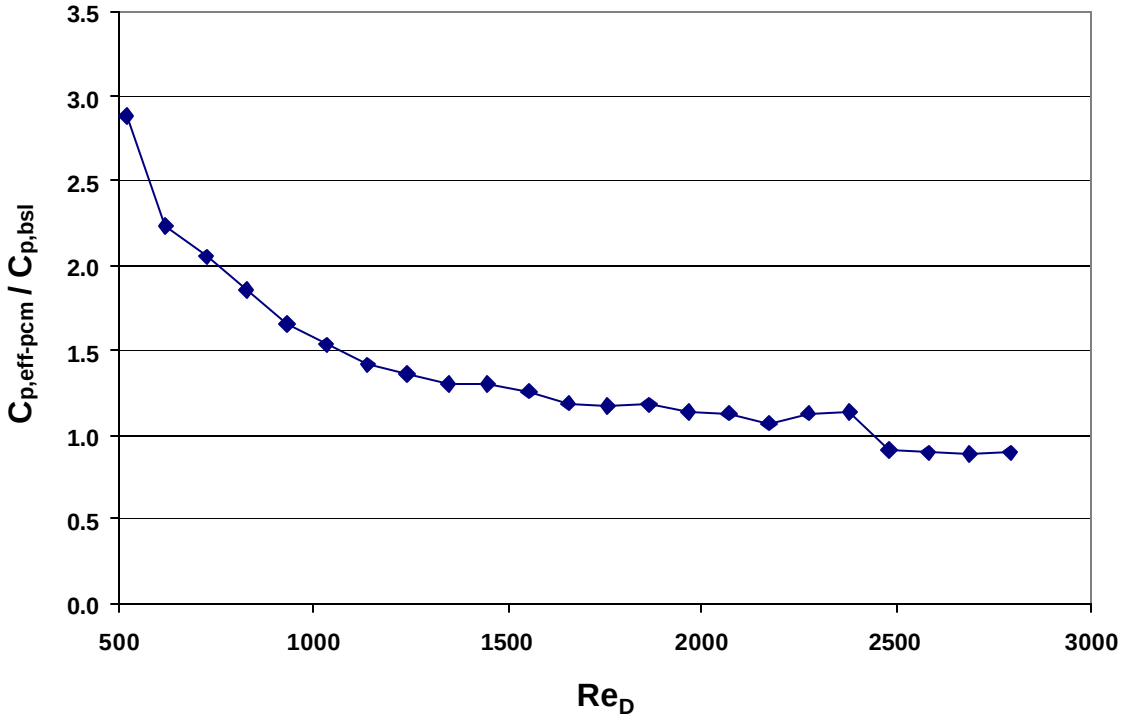

Figure 36: Ratio of effective specific heat versus Re_D

8. CONCLUSION

Results disclosed in this thesis indicate that microencapsulated octacosane PCM fluid is well suited for large scale electronic cooling applications. The fluid was successfully circulated in a liquid pumped loop heat exchanger system, resembling the cooling system of an electric vehicle. Little or no particle breakdown occurred to the encapsulating polymer spheres, as DSC data taken after testing revealed the microPCM fluid had the same heat of fusion as before the test. The high melting point, $T_{melt} \sim 60°C$, of octacosane PCM makes it ideal for cooling electronics such as electric vehicle power transistors and fuel cells. Since the PCM is microencapsulated, the microPCM fluid remains controllable via a pump at all times.

When compared to the baseline 50/50 ethylene-glycol/water fluid, microPCM fluids can provide lower and more uniform wall surface temperatures along sections of a tube with constant heat input. The bulk fluid temperature increase across the heated source of the microPCM fluid is less than the temperature increase of the baseline. Furthermore, the bulk fluid temperature increase across the heat source of the microPCM fluid remains nearly constant, regardless of heat input and flow rate, so long as un-melted PCM particles remain at the exit of the heat source.

Experimental results indicate the microPCM fluid exhibits increased effective specific heat of three times the baseline fluid specific heat. Furthermore, it is expected that even higher effective specific heat values are possible at lower flow rates than those tested, where the specific energy input is pushed above 25 kJ/kg. Calculations estimate the effective specific heat of the 23 percent octacosane microPCM fluid will continue to increase until the specific energy reaches approximately 50 kJ/kg. The effective specific heat should continue

to increase with decreasing mass flow rate until all PCM particles melt across the heated source. This information is encouraging, suggesting that the microPCM fluid performs best when barely pumped through the heated section, minimizing pumping power.

Experimental results show the microPCM fluid exhibits augmented convection heat transfer coefficients over the 50/50 ethylene-glycol/water baseline fluid. The length averaged convection heat transfer coefficient, h_m, increases 20 percent for laminar flow and 30 percent for transitional turbulent flow. Published correlations fit the baseline fluid data well. By using the exit surface thermocouple, T_{s-8}, and the bulk mean fluid temperature, the local convection heat transfer coefficient at the tube exit, $h_{x=1.74}$, is found to increase by 25 percent for laminar flow and up to 60 percent for transitional turbulent flow. Microconvective effects, causing a form of eddy conductivity, are theorized to cause this elevated local convection coefficient during turbulent flow.

To achieve optimum performance from the microPCM fluid, the concentration of solid PCM particles and the mass flow rate must be tailored to the amount of energy that needs to be transferred and the maximum surface temperature at which this can be accomplished. The lower the particle concentration, the less latent heat the fluid can absorb, but also, the lower the viscosity of the microPCM fluid. As the mass flow rate is lowered, pumping power decreases, but surface temperature increases. For the 0.0138 meter diameter, smooth copper tube used in the experiments, the microPCM produced lower exit surface temperatures than the 50/50 baseline fluid for mass flow rates less than 0.035 kg/s. This flow value is independent of the applied heat so long as the concentration of PCM particles is sufficient to have some un-melted particles at the exit of the heat section tube. Calculations suggest that for 600 watts of heat applied to the heat section tube, the microPCM fluid could

be pumped as slow as 0.0125 kg/s before all PCM particles melt. At that mass flow rate the microPCM fluid should only require 0.5 mW of pumping power to cross the heated section.

As high temperature paraffin, octacosane presents itself to many modern electronic cooling applications. MicroPCM fluids should be considered as a working fluid for liquid heat transfer systems when pumping power limitations, low surface temperature or surface temperature uniformity are design requirements. When operated under the correct conditions, the enhanced heat capacity of octacosane microPCM fluid will provide lower and more constant surface temperatures, and require less pumping power than conventional coolants.

9. REFERENCES

1. Rohsenow, W.M., Harnett, J.P., and Ganic, E.N., Handbook of Heat Transfer Applications, Second Edition, McGraw-Hill, New York, 1985.

2. Krum, A., and Sergent, J.E., Thermal Management Handbook for Electronic assemblies, McGraw-Hill, New York, N.Y.1998.

3. Douglas, A.A.H., British Patent No. 398,927 (1933).

4. Newton, A.B., U.S. Patent Nos. 2,342,211 (1944); 2,396,338 (1946).

5. Telkes, M. "Development of High Capacity Heat Storage Materials", Phase I Study of Materials, MIT laboratory R-380, Cambridge, MA, 1962.

6. Bailey, J.A., and Mulligan, J.C., and Liao, C.K., "Research on Solar Energy Storage Subsystems Utilizing the Latent Heat of Phase-Change of Paraffin Hydrocarbons for the Heating and Cooling of Buildings", NSF/RANN Final Report GI-44381, 1977.

7. Bailey, J.A., and Mulligan, J.C., and Liao, C.K., "Research on Solar Energy Storage Subsystems Utilizing the Latent Heat of Phase-Change of Organic Materials", ERDA Final Report EY-76-5-05-5101, 1978.

8. Bailey, J.A., and Mulligan, J.C., Ozisik, M.N., and Maday, C.J., "Demonstration and Evaluation of Phase-Change Thermal-Energy Storage in Residential Heat Pump Systems", Final Report, NCEI-0034, 1981.

9. Colvin, D.P., and Mulligan, J.C., "Investigation and Development of a Phase Change Thermal Energy Storage System Using Microencapsulated Phase Change Materials." Final Report NASA Contract NAS8-35840, 1987.

10. Core, K.L., The use of slurries of microencapsulated phase change materials to enhance heat transfer in liquid-coupled heat exchanger systems, M.S. Thesis, N. C. State University, Raleigh, NC, 1987.

11. Romesburg, L.J., Enhancement of heat transfer in liquids with microencapsulated phase change materials, M.S. Thesis, N. C. State University, Raleigh, NC, 1988.

12. Colvin, D.P., and Mulligan, J.C., "Use of microencapsulated Phase Change Material as a Space Suit Coolant, Final Report," NASA Contract NAS8-35840, NASA Manned Space Craft Center, Huston, 1989.

13. Colvin, D.P., Mulligan, J.C., Bryant, Y.G., and Duncan, J.D., "Microencapsulated Phase Change Material Heat Transfer Systems," USAF Report WRDC TR 89-3072, Wright Research and Development Center, 1989.

14. Colvin, D.P., Mulligan, J.C., Bryant, Y.G., and Gravely, B.G., "Microencapsulated PCM Slurries for Heat Transfer and Energy Storage in Spacecraft Systems," Proc 6th Symposium on Space Nuclear Power Systems, Albuquerque, NM, 1989.

15. Colvin, D.P., Mulligan, J.C., and Bryant, Y.G., "Enhanced Heat Transfer in Environmental Systems Using Microencapsulated Phase Change Materials," SAE Paper No. 921224, 22nd Conference on Environmental Systems, Seattle, WA, 1992.

16. Mulligan, J.C., Colvin, D.P., and Bryant, Y.G., "Use of Two-Component Fluids of Microencapsulated Phase-Change Materials for Heat Transfer in Spacecraft Thermal Systems," AIAA Paper No. 94-2004, 6th AIAA/ASME Joint Thermophysics and Heat Transfer Conf, Colorado Springs, CO, 1994, published in J. Spacecraft and Rockets, Vol 33, No. 2, 1996, pp 278-285.

17. Boyer, D., A Numerical Model of a Suspension Containing Microencapsulated Phase Change Material Flowing Through a Tube Using the Enthalpy Method, M.S. Thesis, N. C. State University, Raleigh, NC, 1997.

18. Roy, S.K., and Sengupta, S., "The Melting Process Within Spherical Enclosures", University of Miami, ASME Journal of Heat Transfer, Vol. 109, pp 460-462 1987.

19. Kasza, K.E., Chen, M.M., "Improvement of the Performance of Solar Energy or Waste Heat Utilization Sysetms by Using Phase-Change PCM fluid as an Enhanced Heat-Transfer Storage Fluid", Journal of Solar Energy Engineering, Vol. 107, pp.229-236, August 1985.

20. Charunyakorn, P., Sengupta, S., and Roy, S.K., "Forced convection heat transfer in microencapsulated phase change material slurries: flow in circular ducts", International Journal of Heat and Mass Transfer, Vol 34, No. 3, pp. 819-833, University of Miami, Coral Gables, Fl 33124, Pergamon Press, 1991.

21. Manish, G., Roy, S.K., and Sengupta, S., "Laminar forced convection phase change material suspensions", International Journal of Heat and Mass Transfer, Vol 37, No. 4, pp. 593-604, University of Miami, Coral Gables, Fl 33124, 1994.

22. Fossett, A.J. and Maguire, M.T., "Avionics Passive Cooling With Microencapsulated Phase Change Materials", Transactions of the ASME, Vol. 120, September 1998.

23. Yasushi, Y., Hiromi, T., and Naoyuki, K., "Characteristics of Microencapsulated PCM PCM fluid as a Heat-Transfer Fluid", AIChE Journal, Vol. 45, No. 4, April 1999.

24. AIChE (1985) "Data Complilation Tables of Properties of Pure Compounds," Department of Chemical Engineering, Penn State University.

25. Wallis, G.B., One-Dimensional Two-Phase Flow, McGraw-Hill, New York, 1969.

26. Schlichting, Hermann, Boundary-Layer Theory, McGraw-Hill, New York, 1987, pp 85.

27. Incropera, F.P. and DeWitt, D.P., Introduction to Heat Transfer, Third edition, John Wiley & Sons, New York, NY, p.413, 1996.

28. Eckert, E.R. and Drake, R.M., Analysis of Heat and Mass Transfer, Hemisphere Publishing Corp, New York, N.Y., 1987, p341.

29. Sherwood, Kiley, and Mangsen, *Ibid.*, 24., p. 273, 1932.

30. Sieder, E.N. and Tate, C.E., "Heat Transfer and Pressure Drop of Liquids in Tubes," *Ind. Eng. Chem.*, 28, 1936, pp.1429-1435.

31. Dalle Donne, M. and Bowditch, F. H., "High Temperature Heat Transfer, *Nuclear Engineering*, 8, pp. 20-29, 1963.

32. Collingham, R.E., Blackshear, P.L., and Eckert, E.R., "Mass Transfer in Flowing Laminar Suspensions", Heat Transfer 1970; Proc. of the fourth International Heat Transfer Conference, Paris-Versailles, 1970, V.7, CT2.2.

10. APPENDIX

101(W)	102(W)	103(LBP	104(C)	105(PSA)	106(PSI)	107(C)	108(C)	109(C)	110(C)	111(C)	112(C)	113(C)	114(C)	115(C)	116(C)
298.26	303.37	1.09	58.83	18.52	18.05	78.54	78.14	72.58	84.34	85.41	88.58	92.32	92.28	95.66	95.10
298.15	303.19	1.31	58.90	18.53	18.13	74.97	74.39	71.84	83.74	84.57	87.29	90.42	89.84	92.57	91.66
297.85	302.94	1.53	59.01	18.53	18.15	72.67	72.16	71.29	83.45	84.15	86.64	89.39	88.39	90.78	89.50
296.79	301.89	1.75	59.04	18.53	18.16	70.99	70.43	70.77	83.13	83.77	86.13	88.67	87.40	89.42	87.92
297.14	302.34	1.97	58.87	18.52	18.13	69.54	68.67	70.15	82.79	83.36	85.66	88.03	86.56	88.27	86.58
297.63	302.80	2.19	58.93	18.50	18.13	68.63	67.65	69.88	82.69	83.20	85.46	87.74	86.15	87.74	85.83
298.04	303.24	2.41	58.98	18.51	18.11	67.86	66.84	69.63	82.60	83.11	85.34	87.54	85.86	87.31	85.24
297.63	302.68	2.62	59.04	18.46	18.07	67.37	66.35	69.59	82.85	83.21	85.36	87.50	85.77	87.11	84.82
298.24	303.54	2.84	58.96	18.33	18.04	66.71	65.47	69.12	82.25	82.78	84.86	86.94	85.06	86.36	84.22
297.61	302.92	3.06	58.93	18.31	18.04	66.14	64.89	68.86	82.03	82.59	84.65	86.68	84.76	85.97	83.82
297.72	303.00	3.28	58.93	18.30	18.02	65.67	64.44	68.65	81.83	82.41	84.44	86.44	84.49	85.65	83.49
297.70	303.07	3.50	58.85	18.29	18.00	65.17	63.89	68.36	81.49	82.18	84.19	86.17	84.21	85.29	83.15
296.55	301.71	3.72	59.04	18.32	18.03	65.03	63.77	68.33	81.45	82.17	84.19	86.13	84.16	85.21	83.06
298.13	303.35	3.94	58.75	18.34	18.06	64.41	63.10	67.93	80.97	81.80	83.85	85.77	83.79	84.83	82.53
296.83	301.99	4.15	59.09	16.12	15.86	64.47	62.94	67.97	80.57	81.74	83.87	85.75	83.79	84.80	82.45
297.88	303.00	4.37	59.10	16.53	16.32	64.10	62.81	67.65	80.15	81.36	83.57	85.39	83.40	84.40	82.16
297.51	302.86	4.59	58.82	16.05	15.80	63.74	63.19	67.55	79.55	81.15	83.17	84.72	82.41	82.67	79.44
297.08	302.22	4.81	59.03	16.11	15.84	63.72	63.48	67.58	79.22	80.80	82.46	83.54	81.10	81.43	77.88
297.15	302.64	5.03	58.85	15.77	15.57	63.34	63.02	67.21	78.62	79.27	81.35	82.03	79.59	80.61	77.15
297.46	302.95	5.25	58.77	15.81	15.62	63.10	62.73	67.03	78.20	78.77	80.58	81.42	79.03	80.05	76.58
297.70	303.14	5.47	58.90	15.86	15.65	63.11	62.79	67.12	77.95	78.19	79.63	80.51	78.58	79.69	76.18
296.94	302.39	5.68	58.84	15.89	15.69	62.89	62.53	66.93	77.51	77.41	78.76	79.99	78.07	79.04	75.61
298.20	303.77	5.90	58.85	15.94	15.72	62.79	62.44	66.83	77.23	76.86	78.14	79.75	77.77	78.63	75.14
297.31	302.83	6.12	58.79	16.00	15.78	62.61	62.28	66.69	76.81	76.05	77.54	79.38	77.26	78.05	74.62
298.29	303.70	6.34	58.81	16.07	15.84	62.52	62.17	66.59	76.55	75.56	77.22	79.13	76.91	77.68	74.27
296.43	301.70	6.56	58.85	16.22	15.98	62.46	62.11	66.49	76.22	75.07	76.94	78.77	76.50	77.31	74.07
297.41	302.81	6.78	58.77	16.34	16.08	62.32	61.97	66.36	75.92	74.62	76.68	78.43	76.18	76.94	73.76

Appendix A–1: Steady state for 50/50 ethylene-glycol/water baseline, Q_{supply} = 600 watts.

101(W)	102(W)	103(LBP)	104(C)	105(PSA	106(PSI)	107(C)	108(C)	109(C)	110(C)	111(C)	112(C)	113(C)	114(C)	115(C)	116(C)
250.61	249.77	1.09	58.86	15.24	14.81	75.14	73.49	69.42	80.25	80.52	83.60	86.58	86.40	89.27	87.89
250.78	250.06	1.31	58.90	15.28	14.90	72.33	70.75	68.80	79.87	79.95	82.71	85.25	84.60	87.05	85.27
251.87	251.06	1.53	58.78	15.46	-10.05	70.65	68.99	68.38	79.58	79.57	82.19	84.51	83.56	85.73	83.70
250.80	250.04	1.75	58.84	15.43	-4.85	68.94	67.31	67.90	79.20	79.12	81.60	83.69	82.44	84.30	81.93
251.04	250.33	1.97	58.85	15.45	-6.47	67.67	66.10	67.67	79.04	78.90	81.32	83.27	81.85	83.43	80.85
250.79	250.05	2.19	58.82	15.46	-16.08	67.03	65.50	67.42	78.80	78.64	81.02	82.92	81.41	82.89	80.24
250.38	249.77	2.41	58.89	15.47	-6.47	66.42	64.87	67.30	78.73	78.58	80.93	82.77	81.20	82.57	79.80
250.69	249.98	2.62	58.83	15.49	-4.96	65.82	64.24	67.00	78.47	78.33	80.65	82.46	80.82	82.10	79.28
250.79	250.12	2.84	58.90	15.49	-5.36	65.40	63.93	67.06	78.43	78.33	80.64	82.41	80.75	81.97	79.10
251.48	250.74	3.06	58.83	15.51	13.44	64.92	63.26	66.79	78.27	78.21	80.50	82.26	80.57	81.73	78.83
250.48	249.86	3.28	58.85	15.53	-0.04	64.51	62.80	66.56	77.95	77.96	80.23	81.94	80.24	81.36	78.45
250.22	249.64	3.50	58.85	15.55	15.39	64.17	62.43	66.39	77.69	77.81	80.07	81.77	80.07	81.15	78.22
250.26	249.62	3.72	58.84	15.57	15.40	63.90	62.13	66.24	77.48	77.70	79.96	81.64	79.93	80.97	78.05
250.74	250.13	3.94	58.84	15.60	15.43	63.62	61.82	66.10	77.17	77.58	79.88	81.54	79.81	80.83	77.90
250.63	250.02	4.15	58.81	15.65	15.46	63.42	61.69	65.95	76.88	77.37	79.71	81.34	79.61	80.59	77.68
251.92	251.05	4.37	58.81	15.68	15.48	63.14	61.64	65.92	76.65	77.30	79.68	81.28	79.51	80.45	77.46
251.40	250.66	4.59	58.79	15.73	15.53	62.96	61.78	65.72	76.22	77.02	79.39	80.74	78.83	79.70	76.51
251.05	250.42	4.81	58.81	15.76	15.56	62.83	62.00	65.70	75.98	76.79	79.10	80.29	78.12	78.72	75.62
249.90	249.33	5.03	58.82	15.85	15.63	62.73	62.20	65.57	75.57	76.41	78.65	79.56	77.34	77.92	74.59
250.48	249.85	5.25	58.73	15.64	15.42	62.45	62.13	65.41	75.09	75.84	77.61	78.08	75.93	76.67	73.76
251.60	250.94	5.47	58.78	15.65	15.43	62.47	62.12	65.48	75.10	75.74	77.24	77.70	75.73	76.61	73.68
251.11	250.47	5.68	58.83	15.68	15.45	62.37	62.06	65.41	74.64	74.86	76.02	76.73	75.17	76.05	73.05
249.53	248.85	5.90	58.81	15.70	15.47	62.27	61.97	65.29	74.34	74.33	75.35	76.40	74.79	75.55	72.68
250.16	249.56	6.12	58.85	15.74	15.49	62.20	61.89	65.30	74.10	73.78	74.79	76.16	74.45	75.12	72.32
249.99	249.37	6.34	58.76	15.76	15.50	62.04	61.70	65.24	73.71	73.12	74.32	75.81	74.06	74.71	71.85
250.24	249.60	6.56	58.83	15.80	15.54	62.01	61.67	65.25	73.49	72.64	74.10	75.64	73.77	74.41	71.55
249.34	248.66	6.78	58.86	15.85	15.58	61.97	61.64	65.23	73.26	72.28	73.89	75.38	73.47	74.12	71.26
250.73	250.05	7.00	58.83	16.04	15.79	61.84	61.49	65.24	73.04	71.93	73.70	75.15	73.25	73.88	71.00

Appendix A–2: Steady state for 50/50 ethylene-glycol/water baseline, Q_{supply} = 500 watts.

101(W)	102(W)	103(LBP)	104(C)	105(PSA)	106(PSI)	107(C)	108(C)	109(C)	110(C)	111(C)	112(C)	113(C)	114(C)	115(C)	116(C)
200.74	198.68	1.09	58.93	15.33	14.95	70.95	69.83	67.62	75.76	75.99	78.38	80.63	80.48	82.79	81.76
200.78	198.69	1.31	58.85	15.31	14.97	69.24	68.00	67.11	75.40	75.55	77.70	79.66	79.18	81.08	79.92
201.36	199.22	1.53	58.80	15.31	15.02	67.55	66.37	66.68	75.10	75.16	77.17	78.90	78.13	79.69	78.31
200.64	198.50	1.75	58.90	15.33	15.06	66.40	65.31	66.47	74.88	74.89	76.83	78.40	77.48	78.86	77.27
201.60	199.42	1.97	58.82	15.35	15.09	65.55	64.47	66.22	74.66	74.63	76.56	78.05	77.02	78.19	76.55
201.81	199.58	2.19	58.89	15.40	15.15	64.92	63.78	66.05	74.56	74.51	76.42	77.84	76.73	77.72	76.03
201.76	199.32	2.41	58.83	15.50	15.27	64.35	63.21	65.78	74.32	74.24	76.12	77.49	76.33	77.34	75.49
201.55	199.51	2.62	58.79	15.40	15.17	64.02	62.66	65.64	74.35	74.28	76.12	77.48	76.29	77.18	75.40
202.11	199.81	2.84	58.80	15.42	15.19	63.68	62.26	65.48	74.19	74.17	75.98	77.32	76.10	77.13	75.15
200.97	198.55	3.06	58.88	15.43	15.20	63.55	62.07	65.43	74.10	74.08	75.88	77.19	75.95	76.96	74.98
201.36	199.02	3.28	58.86	15.46	15.23	63.18	61.66	65.24	73.87	73.97	75.74	77.01	75.76	76.74	74.73
201.74	199.39	3.50	58.76	15.56	15.34	62.88	61.28	65.04	73.57	73.76	75.55	76.81	75.57	76.51	74.49
201.76	199.34	3.72	58.79	15.67	15.46	62.67	61.13	64.92	73.32	73.65	75.46	76.68	75.43	76.35	74.35
201.34	198.86	3.94	58.91	15.86	15.66	62.56	60.96	64.86	73.07	73.54	75.38	76.58	75.33	76.24	74.26
201.68	199.42	4.15	58.83	15.71	15.51	62.43	60.84	64.82	73.03	73.57	75.45	76.66	75.37	76.23	74.19
201.88	199.67	4.37	58.84	15.74	15.53	62.26	60.92	64.69	72.71	73.38	75.27	76.39	75.00	75.76	73.59
202.69	200.55	4.59	58.98	15.77	15.56	62.27	61.45	64.77	72.62	73.36	75.24	76.21	74.63	75.10	72.69
201.22	198.95	4.81	58.88	15.78	15.57	62.08	61.45	64.58	72.19	72.89	74.62	75.13	73.32	73.76	71.15
201.47	198.93	5.03	58.87	15.98	15.76	61.89	61.58	64.44	71.64	71.85	72.73	73.35	71.83	72.60	70.27
201.45	199.49	5.25	58.70	15.64	15.44	61.67	61.26	64.09	71.37	72.04	73.60	74.06	72.31	72.90	70.62
201.66	199.49	5.47	58.79	15.69	15.48	61.66	61.48	64.06	70.98	71.28	72.45	73.15	71.37	72.03	69.82
201.01	198.94	5.68	58.84	15.73	15.51	61.58	61.24	64.01	70.92	71.10	72.04	72.62	71.28	71.94	69.68
201.50	199.38	5.90	58.80	15.76	15.54	61.48	61.16	63.93	70.71	70.62	71.44	72.37	71.08	71.66	69.38
201.50	199.27	6.12	58.81	15.80	15.57	61.42	61.08	63.88	70.50	70.16	71.02	72.16	70.82	71.38	69.11
201.53	199.28	6.34	58.83	15.84	15.60	61.36	61.03	63.86	70.26	69.70	70.74	71.99	70.53	71.06	68.82
200.87	198.45	6.56	58.81	15.90	15.65	61.28	60.92	63.78	70.00	69.31	70.45	71.68	70.22	70.71	68.47
200.78	198.38	6.78	58.85	15.94	15.69	61.25	60.90	63.77	69.83	69.02	70.34	71.53	70.03	70.54	68.27
201.80	199.39	7.00	58.86	16.01	14.94	61.20	60.84	63.73	69.66	68.77	70.20	71.31	69.83	70.34	67.98

Appendix A–3: Steady state for 50/50 ethylene-glycol/water baseline, Q_{supply} = 400 watts.

101(W)	102(W)	103(LBP)	104(C)	105(PSA)	106(PSI)	107(C)	108(C)	109(C)	110(C)	111(C)	112(C)	113(C)	114(C)	115(C)	116(C)
296.83	301.78	3.30	58.74	15.69	15.59	61.29	60.09	67.86	79.31	78.89	81.74	83.78	81.78	82.99	80.69
296.72	301.45	3.96	58.88	15.79	15.71	61.23	59.76	67.26	78.97	78.31	80.99	82.91	80.86	81.86	79.58
297.77	302.65	4.62	58.89	15.88	15.81	61.17	59.60	66.92	78.87	78.17	80.76	82.62	80.54	81.49	79.18
296.09	300.92	5.28	59.02	16.00	15.93	61.14	59.55	66.87	78.56	77.93	80.43	82.20	80.11	80.99	78.72
296.16	300.96	5.94	58.96	16.12	16.04	61.07	59.42	66.67	78.29	77.75	80.20	81.90	79.77	80.63	78.37
296.36	301.13	6.60	58.92	16.27	16.15	60.99	59.35	66.50	78.05	77.60	80.03	81.68	79.56	80.38	78.16
297.81	302.72	7.26	58.83	16.42	16.29	60.90	59.20	66.29	77.72	77.42	79.83	81.44	79.28	80.08	77.87
297.76	302.71	7.92	58.82	16.54	16.42	60.84	59.18	66.12	77.45	77.31	79.71	81.28	79.13	79.92	77.72
297.93	302.79	8.58	58.81	16.77	16.68	60.77	59.12	65.98	77.10	77.15	79.54	81.07	78.89	79.63	77.41
297.29	302.16	9.24	58.90	16.97	16.73	60.73	59.18	65.88	76.76	76.98	79.38	80.85	78.65	79.41	77.25
297.15	302.12	9.90	58.93	17.16	16.88	60.69	59.19	65.83	76.49	76.88	79.32	80.77	78.55	79.31	77.15
297.88	302.77	10.56	58.82	17.38	17.05	60.57	59.10	65.69	76.16	76.70	79.18	80.62	78.38	79.11	76.97
298.60	303.36	11.22	58.83	17.60	17.24	60.53	59.10	65.64	75.84	76.53	79.09	80.51	78.25	78.96	76.85
297.09	301.95	11.88	58.97	17.80	17.42	60.54	59.24	65.59	75.53	76.32	78.95	80.37	78.09	78.79	76.70
297.19	302.06	12.54	58.91	18.07	17.63	60.47	59.19	65.53	75.16	76.03	78.74	80.16	77.86	78.53	76.42
297.89	302.78	13.20	58.95	18.32	17.83	60.43	59.28	65.49	74.91	75.83	78.63	80.02	77.64	78.24	76.06
296.98	301.94	13.86	58.80	18.61	18.06	60.31	59.36	65.31	74.42	75.25	77.97	79.16	76.45	76.73	74.33
297.97	303.04	14.52	58.82	18.88	18.28	60.20	59.59	65.41	74.18	75.04	77.31	77.97	74.85	74.97	72.23
297.64	302.70	15.18	58.86	19.23	18.55	60.15	59.80	65.35	73.81	74.55	75.84	76.04	72.88	73.11	70.53
297.58	303.34	15.84	58.83	19.28	-0.59	60.40	60.00	64.90	73.64	73.64	74.98	75.32	72.37	72.59	69.08
297.11	302.60	16.50	58.76	19.55	-6.05	60.32	59.96	64.83	73.28	72.84	73.90	74.68	72.07	72.34	68.79
296.48	302.05	17.16	58.83	19.88	18.87	60.34	59.97	64.83	72.96	72.06	73.12	74.36	71.88	72.01	68.55
296.77	302.34	17.82	58.88	20.23	19.36	60.34	59.96	64.79	72.74	71.51	72.80	74.23	71.64	71.74	68.29

Appendix A–4: Steady state for 23 % octacosane microPCM fluid, Q_{supply} = 600 watts.

101(W)	102(W)	103(LBP)	104(C)	105(PSA)	106(PSI)	107(C)	108(C)	109(C)	110(C)	111(C)	112(C)	113(C)	114(C)	115(C)	116(C)
250.78	249.87	3.30	58.81	15.70	15.50	61.36	60.19	66.22	75.87	75.51	77.72	79.55	77.85	79.08	76.04
251.47	250.62	4.62	58.81	15.91	15.70	61.22	59.70	65.49	75.41	74.88	76.87	78.46	76.58	77.49	74.45
250.98	250.18	6.60	58.87	16.37	16.09	61.00	59.42	65.01	74.72	74.47	76.34	77.77	75.85	76.61	73.65
251.43	250.55	8.58	58.79	16.81	16.49	60.75	59.18	64.60	73.88	74.10	75.99	77.32	75.35	76.03	73.07
250.51	249.72	10.56	58.89	17.48	16.90	60.60	59.16	64.38	73.01	73.63	75.68	76.94	74.94	75.53	72.62
250.96	250.16	12.54	58.84	18.00	17.50	60.43	59.07	64.21	72.20	73.03	75.36	76.65	74.59	75.08	72.16
250.80	249.98	13.86	58.91	18.44	17.93	60.31	59.60	64.14	71.72	72.42	74.70	75.56	72.96	73.00	69.70
250.52	249.93	15.18	58.88	19.00	18.33	60.27	59.86	64.08	71.17	71.40	72.86	73.20	70.53	70.56	67.47
251.20	250.42	15.84	58.82	19.26	18.56	60.22	59.82	64.03	70.93	70.84	71.96	72.35	69.98	70.12	67.12
250.47	249.84	16.50	58.84	19.56	18.80	60.20	59.82	63.98	70.68	70.22	71.11	71.85	69.74	69.90	66.92
251.20	250.51	17.16	58.84	19.85	19.01	60.18	59.81	64.03	70.49	69.72	70.72	71.74	69.66	69.74	66.80
251.14	250.26	17.82	58.75	20.13	19.26	60.10	59.71	63.95	70.28	69.29	70.46	71.59	69.43	69.49	66.59

Appendix A–5: Steady state for 23 % octacosane microPCM fluid, Q_{supply} = 500 watts.

101(W)	102(W)	103(LBP)	104(C)	105(PSA)	106(PSI)	107(C)	108(C)	109(C)	110(C)	111(C)	112(C)	113(C)	114(C)	115(C)	116(C)
201.22	199.29	3.30	58.85	15.64	15.45	61.24	60.07	64.80	72.01	71.64	73.33	74.73	73.33	74.22	71.74
200.59	198.47	4.62	58.89	15.88	15.64	61.05	59.66	64.26	71.60	71.16	72.71	73.94	72.41	73.09	70.61
201.57	199.60	6.60	58.81	16.27	16.02	60.75	59.32	63.91	70.99	70.85	72.30	73.42	71.84	72.39	70.00
201.60	199.41	8.58	58.86	16.74	16.41	60.54	59.23	63.72	70.36	70.60	72.11	73.14	71.54	72.03	69.68
200.68	198.43	10.56	58.89	17.31	16.90	60.39	59.15	63.50	69.63	70.14	71.82	72.79	71.14	71.56	69.28
201.17	199.07	12.54	58.83	17.92	17.42	60.20	59.14	63.30	69.02	69.60	71.47	72.42	70.69	70.97	68.61
201.10	198.93	13.86	58.85	18.36	17.80	60.18	59.55	63.19	68.71	69.16	70.95	71.65	69.60	69.59	67.00
201.01	198.77	15.18	58.89	18.93	18.24	60.14	59.75	63.10	68.36	68.44	69.66	69.93	67.89	67.89	65.52
200.77	198.54	15.84	58.85	19.21	18.47	60.11	59.74	63.03	68.17	68.02	69.01	69.34	67.54	67.65	65.32
200.60	198.41	16.50	58.84	19.52	18.72	60.05	59.70	62.89	68.01	67.63	68.46	69.02	67.38	67.48	65.15
200.95	198.70	17.16	58.87	19.83	18.98	60.03	59.66	62.79	67.84	67.23	68.13	68.86	67.26	67.27	65.00
201.88	199.65	17.82	58.80	20.20	19.30	59.98	59.61	62.73	67.71	66.95	67.97	68.79	67.12	67.16	64.93

Appendix A–6: Steady state for 23 % octacosane microPCM fluid, Q_{supply} = 400 watts.